Influence of pyrolysis temperature on the performance of cotton stalk biochar for hexavalent chromium removal from wastewater

By

Usama Khalid

(00000319290)

A thesis submitted in partial fulfillment of the requirements for the degree of Master of Science in Environmental Engineering

Institute of Environmental Sciences and Engineering,

School of Civil and Environmental Engineering,

National University of Sciences and Technology

Islamabad, Pakistan

(2022)

Influence of pyrolysis temperature on the performance of cotton stalk biochar for hexavalent chromium removal from wastewater

By

Usama Khalid

(00000319290)

A thesis submitted in partial fulfillment of the requirements for the degree of Master of Science

in

Environmental Engineering

Institute of Environmental Sciences and Engineering,

School of Civil and Environmental Engineering,

National University of Sciences and Technology

Islamabad, Pakistan

(2022)

THESIS ACCEPTANCE CERTIFICATE

Certified that the contents and forms of the thesis entitled **"Influence of pyrolysis temperature on the performance of cotton stalk biochar for hexavalent chromium removal from wastewater"** submitted by Mr. Usama Khalid, Registration No. 00000319290 found complete in all respects as per NUST Regulations, are free of plagiarism, errors, and mistakes and is accepted as partial fulfilments for the award of MS degree. It is further certified that necessary amendments as pointed out by GEC members of the scholar have been incorporated in the said thesis.

Supervisor: _____

Dr. Ali Inam

Assistant Professor

IESE, SCEE, NUST

Head of Department: _____

Dr. Muhammad Zeeshan Ali Khan

IESE, SCEE, NUST

Dean/Principal: _____

IESE, SCEE, NUST

CERTIFICATE

It is certified that the contents and forms of the thesis entitled

"Influence of pyrolysis temperature on the performance of cotton stalk biochar for hexavalent chromium removal from wastewater"

Submitted by

Mr. Usama Khalid

Has been found satisfactory for partial requirements of the degree of

Master of Science in Environmental Engineering.

Supervisor: _____

Dr. Muhammad Ali Inam

Assistant Professor

IESE, SCEE, NUST

GEC Member: ……..

Dr. Muhammad Zeeshan Ali Khan

Associate Professor

IESE-SCEE, NUST

GEC Member: ……

Engr. Nida Maqbool

Assistant Professor

IESE-SCEE, NUST

DECLARATION

I certify that this research work titled "**Influence of pyrolysis temperature on the performance of cotton stalk biochar for hexavalent chromium removal from wastewater**" is my own work. The work has not been presented elsewhere for assessment. The material that has been used from other sources as been properly acknowledged.

Usama Khalid

00000319290

DEDICATION

Dedicated to my exceptional parents, adored siblings, and my friends whose tremendous support and cooperation led me to this wonderful accomplishment.

ACKNOWLEDGEMENT

First and foremost, I acknowledge that it is by the grace of **Almighty Allah** that I have been able to complete this manuscript. All respect to the **Holy Prophet (P.B.U.H)** whose life is the model I am trying to base my life around.

Next, I express my utmost thanks to my supervisor **Dr. Muhammad Ali Inam**, who has supported and guided me throughout my research. His keen interest and valuable suggestions have helped me overcome all obstacles encountered during my research work. I will forever be thankful for his incredible guidance, encouragement, and sympathetic attitude during the entire period of my research. I am also thankful for the meaningful advice and inspiring attitudes of **Dr. Zeeshan Ali Khan** and **Engr. Nida Maqbool** which encouraged me to work harder during my research.

This acknowledgement would be incomplete if I do not pay my sincere and heartedly thanks to my cherished and loving parents for their sacrifices, prayers, and affections without which it would have been nearly impossible to achieve my goals. My sincerest thanks to all my friends at IESE specially Usama Jameel & Amir Younus for their support and help during my MS course at NUST. I would also thank other institutes for their continuous support and encouragement throughout my time at NUST. Last but not the least I would like to thank all the laboratory staff at IESE for their help and cooperation.

Usama Khalid.

TABLE OF CONTENTS

LIST OF ABBREVIATIONS

U.S. EPA	United States Environmental Protection Agency
CSB300	Cotton Stalk Biochar prepared at 300 °C
CSB400	Cotton Stalk Biochar prepared at 400 °C
CSB500	Cotton Stalk Biochar prepared at 500 °C
ARCSB300	CSB300 after Cr (VI) removal
ARCSB400	CSB400 after Cr (VI) removal
ARCSB500	CSB500 after Cr (VI) removal

LIST OF TABLES

LIST OF FIGURES

ABSTRACT

In recent years, biochar has gained popularity as green adsorbent when dealing with hexavalent chromium ions in the water environment. Herein, we prepared biochar at distinct pyrolysis temperatures, i.e., 300, 400, and 500 ºC (denoted as CSB300, CSB400, and CSB500, respectively), using cotton stalks as biomass, and we investigated its impact on Cr (VI) removal. The characterization results based on SEM-EDS, BET, CHN, XRD, and FTIR analysis showed that the surface area, surface morphology, and elemental and functional group composition of CSB were considerably influenced by pyrolysis temperature. Despite having the lowest surface area, CSB500 presented superior adsorption performance. Batch sorption experiments with Cr (VI) solutions (20 mg/L) showed the optimal removal conditions to be pH (2), contact time (2 hours), and biochar dosage (3 g/L). Adsorption kinetics and isotherms were well defined by the Pseudo second order and Freundlich model. The thermodynamic studies showed the spontaneous and endothermic nature of the sorption process. The potential Cr (VI) removal mechanism mainly involved electrostatic attraction followed by Cr (VI) reduction to Cr (III) and complexation. Regeneration studies showed that the reusability aspect of the biochar could be improved, while the selected interfering ions had an insignificant effect on CSB500 adsorption capacity.

CHAPTER 1

1 Introduction

1.1 Background

Chromium is a major pollutant in water bodies such as surface water and groundwater due to its carcinogenic, mutagenic, and teratogenic properties (Dong et al., 2011; Mohan et al., 2011). Chromium is discharged into the natural environment from industries like chromate manufacturing, electroplating, metal processing, and leather tanneries (Yang et al., 2021; Zhou et al., 2016). Among the industrial sectors, effluent released from tanneries is considered the primary source of chromium pollution (Tariq et al., 2020). Chromium has varying oxidation states but predominantly exists in hexavalent and trivalent forms (Ma et al., 2014; Rafique et al., 2021). Naturally, Cr (III) exists as insoluble Cr $(OH)_3$, whereas the Cr (VI) ionic species ($HCrO_4^-$, CrO_4^{-2}, CrO_7^{-2}) remain mobile and highly soluble and are 300 times more toxic than Cr (III) (Kimbrough et al., 1999; Shakya and Agarwal, 2019). Therefore, the U.S. EPA (United States Environmental Protection Agency) has set stringent limits (0.05 mg/L) for industries before discharging Cr (VI) into inland surface water (Shakya and Agarwal, 2019). Consequently, the treatment of chromium-rich wastewater has received global attention from the scientific community.

Pakistan has more than 800 tanneries, producing 47.4 million hides per annum, responsible for discharging Cr (VI) into the natural environment (Benjamin and Nishat, 2021). Korangi, a town in Karachi, alone covers one-third of the total leather exports of Pakistan. Approximately 30-40% of the chromium applied in the tanning process remains unconsumed, which runs away with the industrial effluent. As a result, Korangi tanneries discharge wastewater with elevated Cr concentration (13.05 mg/L) to the surrounding environment (Neelam et al., 2018). Similarly, Sheikhupura, Kasur, and Sialkot areas are severely affected due to the release of high Cr-contaminated wastewater (94.9 mg/L, 89.7 mg/L, and 16.7 mg/L, respectively) (Benjamin and Nishat, 2021; Riaz and Zia, 2020). These numbers are alarmingly above the international and national (<1mg/L for total chromium) standards (Neelam et al., 2018). As a result, finding cost-effective and environmentally friendly solutions to the growing problem of chromium in water bodies is necessary.

For decades, many methods have been tested to treat chromium-containing wastewater, including membrane separation, electrolysis, precipitation, and ion exchange, each of which has its advantages and disadvantages (Othmani et al., 2022; Sinha et al., 2022a). However, due to their high costs, energy requirements, or complex working conditions, most of these techniques are not employed on a large scale or commercialized. Among these methods, adsorption is a more effective and economically viable option (Sinha et al., 2022b). The adsorption technology is still developing, and many researchers focus on producing a low-cost, efficient, and effective adsorbent. Biochar is a type of adsorbent produced by pyrolysis under oxygen-limited or oxygen-free conditions at a temperature less than 700 °C (Shakya and Agarwal, 2019; Tytłak et al., 2015). Pyrolysis is a thermochemical conversion method that yields three types of products, biochar, bio-oil, and biogas (Sakhiya et al., 2020). Biochar production from agricultural residues has become common due to the abundance of agricultural waste, ease of production, and lesser energy requirements (Sinha et al., 2022b). Various biomasses, including Eucalyptus bark (Choudhary and Paul, 2018), sugar beet tailings (Dong et al., 2011), pineapple peel (Shakya and Agarwal, 2019), melaleuca diosmifolia leaf (Kuppusamy et al., 2016), and bagasse (Liang et al., 2020), have been pyrolyzed at different temperatures to produce biochar for Cr (VI) adsorption. The Gossypium plant, from which cotton is harvested, is one of the most harvested plants worldwide, with 30 million tons of cotton produced in 2017/18, which yielded 80 million tons of cotton stalks (Al Afif et al., 2020). Pakistan is the 5^{th} largest producer of cotton and the 4^{th} largest exporter (7%) globally (Anwar et al., 2010). Cotton stalks are used as a fuel for cooking or heating purposes in underdeveloped countries, while in developing and developed countries, it is either added to soil, removed from the cropland, or incinerated, causing environmental and health concerns (Al Afif et al., 2020). Therefore, exploring the potential of cotton stalks for biochar production with further application toward chromium adsorption will not only help resolve the feedstocks' disposal issues but will also be beneficial in mitigating associated human health concerns.

Many factors govern biochar's adsorption performance, but the kind of biomass and pyrolysis temperature has the most significant effect (Sinha et al., 2022a). A few studies (Al Afif et al., 2020; Liu et al., 2018; Makavana et al., 2020; Tomczyk et al., 2020) presented the influence of pyrolysis temperature on the characteristics of cotton stalk

biochar (CSB); however, these studies show inconsistent results. Some studies investigated the CSB adsorption performance in heavy metal removal from aqueous environments. For instance, Gao et al. investigated the lead (Pb) ions removal efficiency of CSB at varying pyrolysis temperatures (250 °C-650 °C) and found that 550 °C was the optimal temperature to produce CSB for Pb removal (Gao et al., 2021). Other studies while working on Cr (VI) removal by CSB presented contradictory findings. For example, Ma et al. produced CSB at 400°C for 1 h and found optimal solution pH as 2, pH_{pzc} as 4.8, and the maximum sorption affinity (q_{max}) as 18.77mg/g for Cr (VI). Tariq et al. produced CSB using the same pyrolysis conditions as Ma et al. and found the optimum pH for Cr (VI) adsorption to be 4, pH_{pzc} of 7.8, and q_{max} of 54.95 mg/g (Ma et al., 2019a; Tariq et al., 2020). Besides, the synthesis of engineered CSB for subsequent Cr (VI) removal was comprehensively investigated; however, detailed investigation on optimization of pyrolysis conditions and operating parameters were rarely discussed in those studies. Therefore, to bridge the literature gap in understanding the Cr (VI) adsorption performance of CSB, our study objectives are discussed in the following section.

1.2 Research Objectives

The main objectives of this research are as follow:

1) examine the effect of varying pyrolysis temperature on the surface properties of CSB.

2) compare the Cr (VI) removal potential of produced CSBs.

3) explore the Cr (VI) removal mechanism under systematically designed sorption experiments.

CHAPTER 2

2 Literature Review

2.1 Background

The world population is growing rapidly, and the need for resources is increasing. Humans are consuming resources at an unsustainable rate, which comes at a cost in the form of environmental damage and threat to human health. The natural environment is degrading due to anthropogenic activities polluting the air, land, and water. Soon the world population will reach 8 billion, and none can live without water. Humans need freshwater for drinking and domestic purposes, but agriculture and the industrial sector consume gigantic quantities of water (Kummu et al., 2016). According to the United Nations World Water Development Report, by 2050, approximately 6 billion of the human population will be affected by water scarcity (Boretti and Rosa, 2019). Mismanagement, overexploitation, climate change, and unfair distribution make providing adequate water to the population more challenging than ever.

Industrial discharge into natural waterbodies is also responsible for polluting the ecosystem. The tannery industry alone discharges 3.5 M Mg of solid waste per year, impacting a huge portion of the human population and damaging the natural environment (Famielec and Wieczorek-Ciurowa, 2011). Tanneries waste contains multiple contaminants, including heavy metals, such as cadmium, copper, zinc, nickel, and chromium (Arabi et al., 2021). Such heavy metals can create severe problems for humans and other forms of life.

Chromium (Cr) is one of the heavy metals which in nature is primarily found in rocks and is released from various industries such as metallurgy, textile, mining, cement, and leather tanning to pollute natural waterbodies. According to a study, approximately 30 to 40 percent of the chromium salts utilized in the tanneries are discharged as waste. Although chromium exists in many oxidation states, the two most profound states are trivalent (Cr^{+3}) and hexavalent (Cr^{+6}) forms. The hexavalent form of chromium is more potent than the others. The plant life that grows around the areas containing Cr amasses it, resulting in serious problems to human health. Furthermore, tackling such issues as cleaning water

resources and decontaminating Cr-containing soils requires techniques that are economically feasible, technically sound, and sustainable.

During the last few decades, multiple techniques have emerged to lessen the effect of Cr (VI) by minimizing its discharge into the natural environment, such as ion exchange, electrocoagulation, photocatalysts, membrane separation, and adsorption (Sinha et al., 2022b). All the aforementioned techniques have some advantages and disadvantages, but the one factor that leads to further search for improved technology is the cost factor. Implementing these technologies for heavy metal removal has been expensive (Yusuff et al., 2022). Adsorption is one technique that has proven to be economically feasible and technically efficient. Thus, further efforts are being made to manufacture cost-effective, technically sound, and reusable adsorbents.

Biochar is a type of adsorbent produced via biomass pyrolysis using less energy than activated carbon, as biochar is produced at temperatures less than 700 °C (Shakya and Agarwal, 2019). The abundance of agricultural waste makes it a low-cost adsorbent. Furthermore, biochar is efficient in heavy metal removal from aqueous medium due to which it has gained scientific community's attention.

2.2 Introduction to Chromium

Chromium is an abundant (24^{th} most) heavy metal in the earth's crust that is toxic and is used in a wide range of industries such as electroplating, leather tanning, dyeing, and textile. In nature, a trivalent oxide compound and chromite with a crystalline structure exist (Wang et al., 2019). Also, Cr is found in many oxidation states, but the dominant forms are trivalent (Cr^{+3}) and hexavalent (Cr^{+6}) forms (Wang et al., 2019). The Cr (VI) ions do not occur naturally but are spread to the natural environment (soil and waterbodies) through human-induced activities (Ertani et al., 2017). Although trivalent chromium is essential for organisms, the hexavalent form is toxic (Pagilla and Canter, 1999). International Agency for Research on Cancer (IARC) has termed Cr (VI) as carcinogenic (Sinha et al., 2022b). Exposure to Cr (VI) beyond the allowable limits can result in different diseases such as asthma, skin disease, liver dysfunction, chronic ulcers, and in extreme cases, death (Sinha et al., 2022a). Due to its detrimental effects, the World Health

Organization (WHO) has set a maximum limit of 0.05 mg/L of total chromium in potable water (Yang et al., 2021).

2.3 Sources of Chromium

Chromium is found in the lithosphere, atmosphere, and hydrosphere. Chromium's existence in the three natural resources can be natural or due to anthropogenic activities. Cr can be found in soil or rocks in the form of chromite (Ertani et al., 2017). Chromite ore is formed when magma is cooled to ambient temperature. Chromite ore is a major resource for Cr used in glass polish; lead chromate ($PbCrO_4$) is an essential ore of Cr used in many industrial activities (Reddy et al., 2022). Different rocks contain different quantities of Cr, but ultramafic and basaltic rocks are known to have the highest chromium concentration (0.2-2.4 g/kg). Limestone and sandstone are types of granitic igneous rocks which can transport Cr into natural waterbodies due to erosion or weathering. Limestone and sandstone contain Cr concentration in the range of 0.02 g/kg to 0.2 g/kg (Sinha et al., 2022b). Cr presence in the atmosphere has also been reported, and the cause has been linked to volcanic eruptions and meteoric and windblown dust. Fly ash is a waste produced from coal combustion and is known to be the main concern of Cr concentration in the lithosphere (Nriagu and Pacyna, 1988). The U.S. EPA has reported 0.001-1 g/kg of Cr in the soil. Cr proliferation in the natural environment is also due to the anthropogenic activities such as unregulated discharge from various industries. Annually, manufacturing industries release approximately 17 million kg of Cr into the ecosystem. Metal industries consume 80% of the total Cr used globally (Sinha et al., 2022b).

2.4 Chromium Application

Chromium has a wide range of industrial applications varying from Metallurgy, electroplating, pigments and dyes to wood preservation. Globally approximately 80% of the mined chromium is used in the metallurgy industry because chromium provides resistance to corrosion and enhances the hardness of steel (Barnhart, 1997). Also, adding chromium to steel makes the steel resistant to corrosion and discoloration. Electroplating and addition of chromium to steel are the most used applications of chromium involving metals. Chromic acids are used in decorative electroplating on nickel and 'hard' plating (Lunk, 2015).

2.5 Effects of chromium

Chromium predominantly exists in trivalent (Cr (III)) and hexavalent (Cr (VI)) form which are discharged into the natural environment through anthropogenic activities (Sinha et al., 2022b). Cr (III) in moderate concentration is vital for humans and is also beneficial to plants as it is necessary for lipid and sugar metabolism (Ma et al., 2019b). Plants require less energy for Cr (III) uptake, making it essential biologically and for its physical functioning (Shanker et al., 2005). In comparison, Cr (VI) is toxic because it has non-degradable, carcinogenic and mutagenic properties, and even its discharge in minimal quantities can cause damage to soil, marine life, humans and the ecosystem (Othmani et al., 2022). Cr (VI) is also highly soluble and has the ability to bioaccumulate; due to these factors, it is more toxic than Cr (III) and is responsible for causing diseases in humans such as skin disease, damaging liver and kidney, asthma, skin rash, and in extreme cases, even death (Yusuff et al., 2022). In 2000, a comprehensive study was conducted by Gibb et al., examining in excess of 2000 workers in a chrome industry. This study took cigarette use into account and conclusively proved that Cr (VI) can cause lung cancer, separate from tobacco use (Gibb et al., 2000).

2.6 Technologies for Chromium (VI) Removal

Due to the detrimental effects of Cr (VI), the scientific community looked for methods to treat Cr-containing wastewater. Over the years, multiple techniques have been developed to treat water and wastewater, such as coagulation and flocculation, ion exchange, membrane separation, chemical precipitation, electrocoagulation, and adsorption (Sinha et al., 2022b). The following are some of the methods used to treat Cr-containing water and wastewater:

- Coagulation and flocculation
- Ion exchange
- Membrane technology
- Adsorption

2.6.1 Coagulation and flocculation

To separate the suspended particles, factors like size, shape, and density of the particles are the influencing parameters in coagulation and flocculation processes. Also, solids suspended in the water have identical surface charges, resulting in repulsive electrostatic forces. Coagulants are used to counter the negative charges, which helps neutralize the surface charges, leading to the formation of flocs, which are eventually separated in the sedimentation process (Kerur et al., 2021). In conventional wastewater treatment, the coagulation, flocculation, and sedimentation processes are interdependent, and if the initial process of coagulation is not successful, the forthcoming processes will not work (Kamali et al., 2021).

Coagulants such as sodium citrate and calcium carbonate were useful in Cr (VI) removal, but aluminum sulphate and ferric chloride were the most efficient due to Cr $(OH)_3$ and Fe $(OH)_3$ precipitation removing up to 99.9% in the process (Sinha et al., 2022b). Furthermore, Fe (II) sulphate completely removed Cr from the system by forming precipitates of Cr $(OH)_3$, and although some of these coagulants are efficient in removing Cr from wastewater, safe disposal of the byproducts of the coagulation process is still a concern (López-Maldonado et al., 2014).

2.6.2 Ion exchange

Ion exchange is another physicochemical technique used for Cr removal that has grasped the attention of the scientific community due to its impressive results. Therefore, in recent years, abundant studies have focused on improving this method using different ion exchange resins (Owlad et al., 2009). Ion Exchange resins consist of granular, ketonic materials with a chemical structure that supports the trade of ions that are either acidic or basic. Thus, solute ions with a similar charge, when in contact with the radicals, substitute any positive or negative ions that were previously present on their surfaces (Kerur et al., 2021). Although the sludge production in the ion exchange process is relatively low, regeneration using chemicals, high quantity of backwash water, and high expenses are some of the disadvantages of this process due to which its use is limited on an industrial scale (Azimi et al., 2017).

2.6.3 Membrane Technology

Membrane technology uses the concept of a pressure gradient to treat water or wastewater. Membrane filtration can remove contaminants ranging from organic and inorganic matter to heavy metals (Owlad et al., 2009). The process of contaminant removal is dependent on factors such as the size of particles, contaminant concentration in solution, pH of a solution, the pore size of the membrane, and pressure gradient (Van der Bruggen et al., 2003). Membranes are manufactured from different materials but most commonly used are ceramic or polymer-built membranes. The size of the particle is not the leading factor in the removal process, as the strong intermolecular interactions between the membrane and the heavy metal ions influence the separation process (Kerur et al., 2021). Polymeric membranes are in demand because of their strength, hydrophobic nature, and they are resistant to chemicals, while ceramic membranes are relatively less strong and costly (Van der Bruggen et al., 2003). Membrane technology has long been used for filtration of water and wastewater because of its ease of operation, and less area needed to operate, but a major disadvantage of this technology is that the membranes require frequent cleaning (Elwakeel et al., 2020).

Following are the filtration processes used for specific purposes depending on the pore size of the membranes:

2.6.3.1 Microfiltration (MF)

Industrial effluents have a varying size of contaminants; microfiltration is used as a pretreatment that helps in removing particles with comparatively bigger sizes (0.1-1 µm). Although microfiltration membranes can take up large quantities of filtrates, clogging and frequent backwashing is still concerning. Microfiltration operates in both end and cross-flow modes (Kerur et al., 2021).

2.6.3.2 Ultrafiltration (UF)

Ultrafiltration uses the electrostatic phenomenon to remove particle sizes in the range of 0.01 to 0.1 µm. Although UF is efficient in removing some pollutants, its pore size is still larger than the size of metal ions; resultingly, it allows the metal ions to go through. Therefore, UF should be used alongside other treatment techniques or membranes with finer pore sizes (Kerur et al., 2021).

2.6.3.3 Nanofiltration (NF)

Because the microfiltration and ultrafiltration members have smaller pore sizes than metal ions and due to the increasingly strict environmental standards, improved membranes with finer pore sizes were required. NF gained widespread attention and is used to treat water, wastewater, and for desalination purposes. Due to its higher flux and less energy requirement, nanofiltration has even replaced RO membranes in some applications (Mulyanti and Susanto, 2018). NF is a suitable technique for removing heavy metals such as Cr, Ni, and As from industrial discharge (Khulbe and Matsuura, 2018).

2.6.3.4 Reverse Osmosis (RO)

RO technology uses permeable or semi-permeable membranes (0.1 – 1 nm) to separate ions, undesirable molecules, and larger particles by overcoming the osmotic pressure by applying pressure, permitting only water molecules in the process. RO applications are gaining attention due to their effectiveness, removing all sorts of molecules, including heavy metals, but the most wide use of RO technology is desalination (Kerur et al., 2021).

2.6.4 Adsorption

The adsorption technique for heavy metal removal has gained widespread attention due to the easy production of adsorbents, better reusability and low cost, less production of byproducts, and easier disposal methods compared to other techniques (Gupta et al., 2021). Due to its advantages, it has been the leading process in removing heavy metals from wastewater.

Adsorption is a phenomenon where the desirable contaminant to remove from a solution is adsorbed onto the surface of an adsorbent (Owlad et al., 2009). Factors such as cost-effectiveness, surface area, and surface functional groups influence the performance of an adsorbent (Shakya and Agarwal, 2019). To make the adsorption process efficient and effective for heavy metal removal, multiple adsorbent materials have been produced from natural or synthetic materials, such as activated carbon, biosorbents, graphene, zeolites, and chitosan. Natural adsorbents are much more cost-effective than commercially available adsorbents because of the abundance of natural waste, such as agricultural waste (Renu et al., 2016).

In the Following section some of the widely used adsorbents are discussed:

2.6.4.1 Activated carbon

Activated carbon has been manufactured since the early 20th century from materials with high carbon content at temperatures greater than 700 °C (Renu et al., 2016). Activated carbon has been used to remove heavy metals and is efficient in decontaminating Cr-containing solutions due to its pore structures and high surface area (Anirudhan and Sreekumari, 2011). To improve the porous structure and increase its surface area, different feedstocks, synthetic materials, and chemical methods have been experimented with and used for removing different kinds of pollutants (Gupta et al., 2021).

2.6.4.2 Carbon nanotubes

The element carbon can exist in various molecular forms known as allotropes. Carbon nanotubes have a high surface area, excellent chemical and physical stability, and well-developed porous structure, which can be further enhanced by chemical activation methods (Gupta et al., 2011). Due to these properties, carbon nanotubes have shown excellent adsorption properties. For instance, Hu et al. produced carbon nanotubes that removed 100% chromium, while Gupta et al. modified carbon nanotubes chemically and achieved 88% chromium removal at pH 6, where chromium adsorption is not favored (Gupta et al., 2011; Hu et al., 2009).

2.6.4.3 Graphene

Graphene is a two-dimensional nanomaterial made from carbon-based materials. It is used for heavy metals removal from aqueous solutions due to its large surface area, physical and chemical stability, well-developed pores, and rich surface functional groups (Gupta et al., 2021). Graphene oxide (GO), a common graphene derivative, consists of the previously mentioned properties and has shown promise in the decontamination of heavy metals such as lead, copper, and chromium from wastewater (Gupta et al., 2011).

2.6.4.4 Biochar

Biochar is a type of adsorbent produced by pyrolysis under oxygen-limited or oxygen-free conditions at a temperature less than 700 °C (Shakya and Agarwal, 2019; Tytłak et al., 2015). The International Biochar Initiative (IBI) defines biochar as “a carbon-rich solid

material obtained from biomass thermochemical conversion under oxygen-free conditions" (Sakhiya et al., 2020). Pyrolysis is a thermochemical conversion method that yields three types of products, biochar, bio-oil, and biogas (Sakhiya et al., 2020). Biochar adsorbents are still developing as many researchers focus on producing low-cost, efficient, and effective adsorbents. Biochar production from agricultural residues has become common due to the abundance of agricultural waste, ease of production, and lesser energy requirements (Sinha et al., 2022b).

Biochar has gained widespread attention due to its use in different fields, such as water and wastewater treatment, enhancing soil fertility, and carbon sequestration. Nevertheless, the effectiveness and efficiency of biochar applications are based on their physicochemical properties, including pH, active sites, and rich surface functional groups. As the biochar technique developed, improving its surface characteristic became the focus of several studies. Many chemical and physical activation methods have been tested over time to improve the physicochemical properties of different biochar prepared using different feedstocks and varying pyrolysis temperatures, as these two factors are dominant in determining the efficiency of biochar.

Biochar technique has been used for Cr (VI) removal from aqueous solution due to its low-cost, ease of production, low energy requirements, effectiveness, and efficiency. For instance, Ma et al. produced raw and chemically modified biochar from cotton stalks for Cr (VI) removal at a pyrolysis temperature of 500 °C with 1 hour contact time. Their batch experiments showed that the adsorption capacity for raw biochar (18.77 mg/g) was lower than the modified biochar (20.05 mg/g) (Ma et al., 2019a). Wang et al. used maize straw as feedstock for biochar production and investigated the effect of pyrolysis temperature (300-600 °C) on the Cr (VI) removal performance of the produced biochar. The experimental results indicated that the biochar produced at lower temperatures was more efficient (adsorption capacity, 91 mg/g) than the ones produced at a higher temperature. Also, the pH of the solution was an important factor in determining the Cr (VI) removal efficiency because as the solution pH increased from 2-8, the removal efficiency decreased considerably. Whereas the maximum Cr (VI) decontamination (>99.9 %) occurred at pH 2. The characterization tools showed that the surface functional groups such as C=O, -CH_2

and -CH_3 groups played a vital role in the adsorption process (Wang et al., 2019). A study was conducted on pineapple peel derived biochar at varying temperatures, and the results suggested that lower pyrolysis temperature was better for biochar produced for Cr (VI) removal. Also, the characterization of the produced biochar showed that surface area was not the dominant factor in determining the biochar performance; instead, rich functional groups on the biochar surface played an influential role (Shakya and Agarwal, 2019). Therefore, the production of low-cost, effective, and efficient biochars has gained attention because it has shown promise in decontamination of heavy metals from water and wastewater.

CHAPTER 3

3 Materials and Methods

In this chapter, the preparation of the feedstock, the biochar production process, characterization, and the factors affecting the removal of chromium (VI) are all covered in detail. In-depth explanations will also be provided for the analytical techniques used for biochar characterization as well as the simulation models applied to quantify the experimental results.

3.1 Feedstock and stock solution preparation

Cotton stalks (CS) were obtained from agricultural land in Multan, Punjab province, Pakistan. Distilled water was used to wash out contaminants like dust and sand particles from the collected feedstock. It was then kept under the sun for seven days to minimize the moisture content. The dried material was ground into smaller uniform particles and passed through sieves from 0.25mm to 2 mm. The particles size less than 0.25mm were used to produce biochar, and the rest were discarded. Stock solution (500mg/l) was prepared by mixing 1.414g of potassium dichromate ($K_2Cr_2O_7$, analytical grade) in 1000ml deionized water. Afterwards, extracts from the stock solutions were diluted according to the need for each experimental run.

3.2 Experimental Setup and Pyrolysis procedure

Following are the parts of the pyrolysis reactor setup, whereas Fig. 1 shows the image of the pyrolysis setup used for biochar production.

1. Fixed Bed reactor
2. Condensers
3. PID temperature controller
4. Flow meter for Nitrogen
5. Heaters

6. Nitrogen cylinder

7. Thermocouples

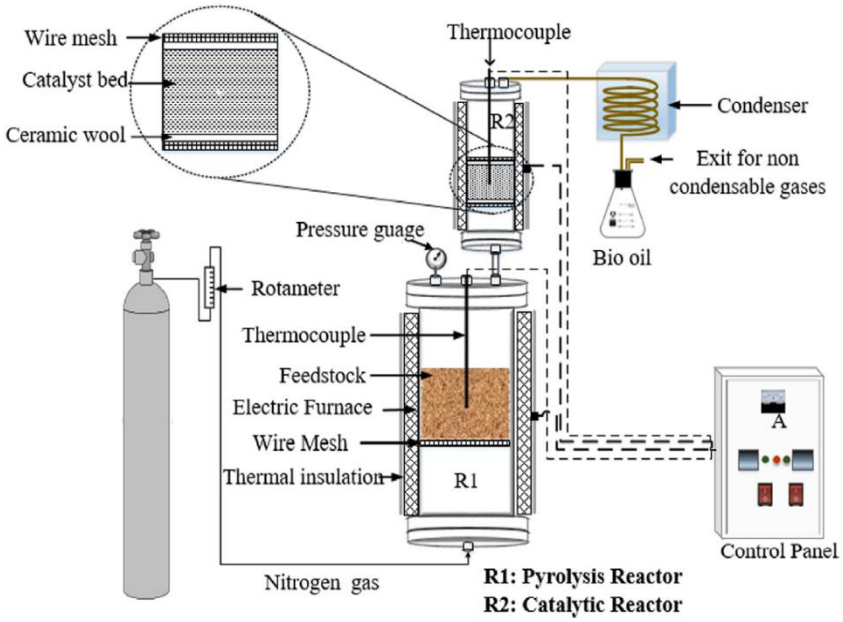

Figure 1. Pyrolysis reactor

The fixed bed reactor was manufactured from stainless steel, the length of which was 20 inches, whereas the internal and external diameters were kept at approximately 4 and 4.5 inches, respectively. The feedstock was kept in the fixed bed reactor for pyrolysis. 100g of biomass was used for each batch run. The heaters were attached outside the reactor with PID temperature controlling the heating rate. Three different temperatures were selected to produce biochar, 300°C, 400°C, and 500°C, denoted as CSB300, CSB400, and CSB500. Nitrogen gas was purged at 600 ml/min from the bottom of the reactor for 30 mins to create an inert environment. Afterward, it was maintained at 50 ml/min throughout the heating process. The temperature was raised to the desired pyrolysis temperature at 20°C/min and maintained for 2 hours. After 2 hours, the heater was turned off, and the N_2 flow increased to 1000ml/min for 10 min to remove the gases in the reactor. A condenser was attached to

the reactor through a pipe from the top of the reactor. The gases and vapors produced during the pyrolysis process would flow through the pipes. When the condensable hot gases flow through the condenser, the gases will condense to produce Bio-oil. The produced Bio-oil was collected in a conical flask which was connected to the condenser. The non-condensable gases would flow through the condenser, into the conical flask, and through the exhaust pipe into the atmosphere. Finally, the produced biochar was collected and stored in airtight plastic bags when the reactor's temperature returned to ambient temperature.

3.3 Yield of the pyrolysis products

The pyrolysis process yields three products, biochar, bio-oil, and biogas (Sakhiya et al., 2020). The following equations were used to determine the yield of the three products.

$$\text{Biochar yield (\%)} = \left(\frac{\text{biochar weight}}{\text{biomass weight}}\right) \times 100 \qquad \textit{Eq. 1}$$

$$\text{Bio-oil Yield (\%)} = \left(\frac{\text{bio-oil weight}}{\text{biomass weight}}\right) \times 100 \qquad \textit{Eq. 2}$$

$$\text{Biogas yield (\%)} = 100 - \text{Biochar (\%)} - \text{Bio-oil (\%)} \qquad \textit{Eq. 3}$$

3.4 Characterization of Feedstock and Cotton Stalk Biochar

The following sections will describe the experimental conditions for proximate analysis and the many characterization tools used to understand the adsorption behavior of CSB.

Proximate Analysis

The feedstock and the prepared biochars' proximate analysis were done following ASTM D3173, D3174, and D3175 methods for moisture, volatile, and Ash content, respectively. The following equation determined the Fixed Carbon (FC).

$$FC = 100 - \text{moisture content (\%)} + \text{ash content (\%)} + \text{volatile matter (\%)} \quad \textit{Eq. 4}$$

To determine moisture content, initially, the samples were placed in an oven using a petri dish for 24 hours at 105°C. After 24 hours, the samples were taken out, and the weight before and after placing them in the oven indicates the moisture content.

To determine the volatile matter, the samples were kept in a muffle furnace using crucibles covered with caps at a constant temperature of 950°C for seven minutes. The samples were taken out, and the difference between the samples' initial and final weight shows volatile matter.

To determine the Ash content, the samples were kept in a muffle furnace using crucibles covered with caps at a constant temperature of 725°C for 3 hours. Afterward, the samples were weighed, and the difference implied the ash content.

3.4.1 Ultimate Analysis

An elemental analyzer (ECS 8020, NC Technologies, Italy) was used to conduct the feedstock and the prepared biochars' elemental analysis (C, H, and N). The following equation determined the oxygen content.

$$\text{Oxygen content} = 100 - (C + H + N + \text{ash content (\%)}) \quad \textit{Eq. 5}$$

3.4.2 Thermogravimetric analysis

Feedstock's thermogravimetric analysis was conducted using an automatic thermogravimetric analyzer (TGA 5500, TA instruments, USA) to understand the thermal decomposition behavior during pyrolysis.

3.4.3 SEM-EDS

The surface morphological study of all three raw biochars and for CSB500 after Cr (VI) removal (ARCSB500) was conducted by using Scanning electron microscopy coupled with energy dispersive spectroscopy (SEM, JSM-6490 A, JEOL Japan).

3.4.4 BET analysis

The surface area and pore size analyzer (NOVA 2200e, Quantachrome Instruments, USA) was used to determine the BET surface properties (quantified based on N_2 multilayer adsorption) of the produced adsorbents.

3.4.5 X- ray diffraction (XRD) spectroscopy

X-ray diffraction (XRD) analysis of the produced biochars before and after Cr (VI) removal was carried out by using X-ray diffractometer equipped with Cu Kα radiation operated at 45 KV and 30 mA (STOE S/N 65022, Germany).

3.4.6 Fourier infrared spectroscopy (FTIR)

The bonding features were examined using Fourier infrared spectroscopy (FTIR, Perkin Elmer Spectrum 10 D, USA)) in the range of 4000-400 cm^{-1} with a resolution of 1 cm^{-1}.

3.4.7 pH and Point of Zero Charge (pH_{PZC})

Feedstock and the prepared biochars pH were measured by mixing samples with deionized water at a weight-to-volume ratio of 1:10 using a multi-meter (WA-2015, Lutron, Taiwan) (Zhou et al., 2016). The method described by (Mortazavian et al., 2018) was used to determine the Point of Zero Charge (pH_{PZC}). In brief, 0.1 g of adsorbent was added to 45ml of 0.1M NaCl solution in 8 different flasks. 0.1M HCL and 0.1M NaOH solutions were used to adjust the pH in each flask to 2.0, 3.0,4.0,5.0,6.0,7.0,8.0, and 9.0. The samples were

placed on a mechanical shaker for 24 hours. The samples were taken off after 24 hours, and the pH was measured using a pH meter. The point on the graphical plot where the initial (x-axis) and equilibrium pH (y-axis) intersect is the point of zero charge.

3.5 Batch adsorption experimental conditions

The series of batch sorption experiments were conducted to explore Cr (VI) removal potential using an orbital shaking incubator (LSI-3016A, DAIHAN LABTECH, Korea) with a mixing speed of 200 rpm. Initially, the influence of CSB dosage (1 to 5 g/L) was examined with 20 mg/L Cr (VI), pH of 2, and 2hrs contact time. Afterwards, pH was varied from 2-9 with Cr (VI) concentration of 20mg/L, CSB dosage (3g/L), and contact time of 2hrs to examine the solution's pH influence on the adsorption process. The 20 mg/L Cr (VI) concentration with pH 2, dosage 3 g/L, and a 5-240 mins time interval was selected to study the kinetics. For adsorption isotherms, varying temperatures (15, 25, and 35°C) and solutions with varying initial Cr (VI) concentration (10-100 mg/L) were mixed for 2hrs with pH kept at 2 and a dosage of 3g/L. The pH was adjusted using 0.1M NaOH and 0.1M HCL solutions.

The removal efficiency (%), equilibrium adsorption capacity (q_e, mg/g), and the adsorption capacity at different times t (q_t, mg/g) were calculated as follows:

$R(\%) = \frac{(C_o - C_t)}{C_o} \times 100$	Eq. 9
$q_e = (C_o - C_e) \times \frac{V}{m}$	Eq. 10
$qt = (C_o - C_t) \times \frac{V}{m}$	Eq. 11

Where R (%) is the adsorbent's Cr (VI) removal efficiency, C_o, C_e, and C_t (mg/L) represents the Cr (VI) concentration at the initial phase, equilibrium phase, and time interval t, V (L) is the solutions volume and m (g) represent the adsorbent mass. Each experiment was repeated twice, and the average values were reported with +/- standard deviations.

3.6 Kinetics Studies

Kinetics experiments were performed with an initial Cr (VI) concentration 20 mg/L for 2 hours during which samples were analyzed at different time intervals (30, 60, 90, and 120 mins). To simulate the kinetic behavior of CSB500, the most frequently used kinetic models, i.e., pseudo-second order (PSO) and pseudo-first order (PFO) were employed. The following section provide details into the non-linear equations of both models.

3.6.1 PFO and PSO kinetic models

The PFO assumes that the rate of change of solute uptake with time is directly proportional to difference in saturation concentration and the amount of solid uptake with time, which is generally applicable over the initial stage of an adsorption process. Whereas the PSO kinetic model assume that the rate limiting step is chemical sorption over sharing or exchanging of electrons between adsorbate and polar functional groups on adsorbent.

The non-linear forms of both PFO and PSO kinetic models are as follows:

Pseudo first order equation: $$q_t = q_e (1- e^{-k1t}) \quad \text{(Eq. 12)}$$

Pseudo second-order equation: $$q_t = q_e^2 k_2 t/(1+q_e k_2 t) \quad \text{(Eq. 13)}$$

Where q_e and q_t, both in (mg/g), represent the amount of adsorbate adsorbed at equilibrium and at the time (t), respectively. K_1 represents the first order (min^{-1}), and K_2 represents the second-order ($g.mg^{-1}.min^{-1}$) rate constant.

3.7 Isotherms studies

Isotherms studies were conducted under three different temperatures, i.e., 15°C, 25°C, and 35°C with initial Cr (VI) concentration of 20mg/l. The optimal values of pH and dosage of

adsorbent were selected i.e., 2.0 and 3.0 g/L respectively. The samples were placed on a shaker at 200 rpm. The contact time selected was also the equilibrium time, i.e., 2hrs.

Freundlich and Langmuir isotherm models were applied to quantify the adsorption data, predicting the multilayer and single layer adsorption, respectively.

3.7.1 Langmuir isotherm model

Langmuir isotherm model is one of the widely used models that describes the correlation between the amount of solute adsorbed on the adsorbent (mg/g) against the solute concentration (mg/L) in the solution at equilibrium condition. This model assumes that monolayer solute adsorption occurs at a fixed number of adsorption sites distributed homogeneously over the adsorbent surface. It is also assumed that these sites have equal affinity for the adsorbate. The non-linear equation describing the model is given as follows:

$$q_e = q_{max} K_L C_e / (1 + K_L C_e) \quad \text{(Eq. 14)}$$

where q_{max} (mg/g) represents the theoretical maximum adsorption capacity, Ce (mg/L) is the equilibrium concentration, q_e (mg/g) is the equilibrium adsorption capacity, K_L (L/mg) is the isotherm constant.

3.7.2 Freundlich isotherm model

Freundlich isotherm model assumes that the adsorption sites have a varied affinity for the adsorbate, and solute adsorption occurs on a heterogeneous surface in the form of multilayers. The non-linear form of the model is given as follows:

$$q_e = K_F C_e^{1/nF} \quad \text{(Eq. 15)}$$

q_e (mg/g) is the equilibrium adsorption capacity, nF is the Freundlich exponent, and K_F is the Freundlich constant.

3.8 Thermodynamic Studies

The thermodynamic parameters, including ΔG°, ΔH°, and ΔS° for Cr (VI) removal by CSB500, were evaluated using the following equations:

$$\Delta G^\circ = -R*T*\ln KL \quad \text{(Eq. 16)}$$

$$\ln KL = (\Delta H^\circ/R)\,(1/T) + (\Delta S^\circ/R) \quad \text{(Eq. 17)}$$

Where T (K) is the solution's temperature, R (8.314 J/mol-K) is the gas constant, and K_L is the Langmuir isotherm constant. The linear van 't Hoff plot of ln K_L versus 1/T gives slope and intercept to determine the value of ΔH° and ΔS°, respectively. ΔG° (kJ/mol) is the change of free energy, ΔS° (J/mol-K) is the change of entropy, and ΔH° (kJ/mol) is the change of enthalpy.

3.9 Regeneration Experiments

The regeneration experiments for CSB500 were performed in three adsorption/desorption cycles. Herein, we added 3g/L of CSB500 in 20 mg/L Cr (VI) suspension after maintaining the working solutions' pH (2), then mixed (200 rpm) for 2 hours at 25°C. The post-adsorption CSB500 was regenerated by adding 3g/L in a regenerating agent (1 M NaOH) solution for 3hrs in a mechanical shaker at 200rpm. The regenerated CSB500 was then used for the next cycle, performed under the same working conditions as the first sequence.

3.10 Interfering ions

One of the objectives was to see the practical applicability of the adsorbent by examining the influence of foreign ions on the absorbent's performance. The experiments were performed in optimal conditions (pH 2, 20mg/L Cr (VI), dosage=3g/l, contact time 2hrs, 200 rpm). Some of the most found ions in wastewater of tannery, dyeing, electroplating industries, or domestic wastewater, such as Phosphate, Sulphate, Chloride, and Nitrate, were added (100mg/L) to Cr (VI) solutions (20 mg/L). The solutions were prepared by adding only one compound of the foreign ions to Cr (VI) solution. These binary

546 mixtures were then tested to assess the sorption affinity of CSB500 towards Cr (VI)
547 species.

CHAPTER 4

4 Results and Discussion

4.1 Determination of Chromium (VI)

After equilibration, each sample was vacuum filtered, to which 1,5-diphenylcarbazide (2% by volume) was added. The supernatant Cr (VI) concentration was measured by reading the absorbance (540 nm using an Ultraviolet-visible spectrophotometer (SPECORD 200 Plus, Analytik Jena, Germany)) of the complex formed from 1,5-diphenycarbazide addition. For such purpose, a standard equation was developed using Cr (VI) solutions (0.1 mg/L to 1 mg/L) by making a calibration curve (R^2>0.999) as presented in the Fig. 2.

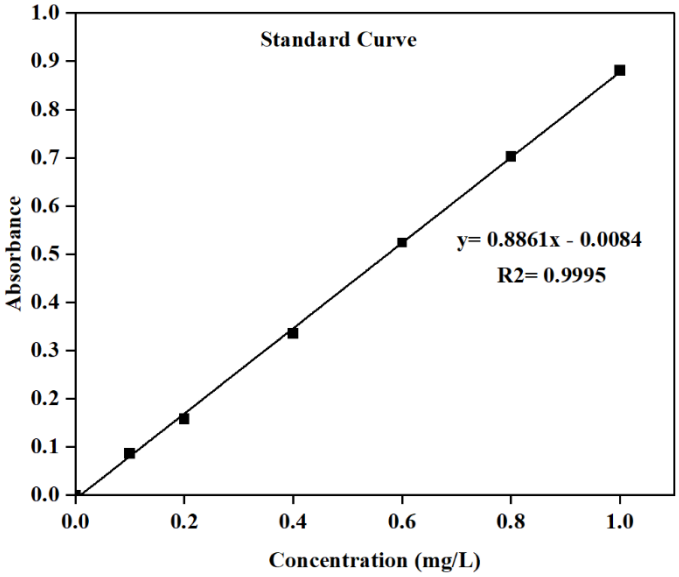

Figure 2. Standard Curve

4.2 Characterization

This section provides detailed insights into the effect of varying pyrolysis temperature on biochars' surface properties before and after interaction with hexavalent chromium species. Table 1 presents a detailed overview of the yield of pyrolysis products, proximate, ultimate analysis, pHpzc, and BET surface properties of feedstock (cotton stalk) and biochar.

4.2.1 Yield of Pyrolysis Products

The results in Table 1 show the impact of varying pyrolysis temperatures on the biochar, bio-oil, and biogas yield. The biochar yield decreases with increased temperature, while bio-oil and biogas yield increases. These trends could be due to the fact that the raw cotton stalk is composed of cellulose, hemicellulose, and lignin which generally degrades at temperatures ranging from 240 to 500 °C and are discharged as gases and volatiles (Al Afif et al., 2020). The gradual degradation of the organic components of the feedstock with increasing temperature causes more biogas yield because more volatile matter turns into gases such as methane, hydrogen, carbon dioxide, and carbon monoxide, resulting in lower biochar yield (Al-Wabel et al., 2013; Usman et al., 2015). At lower temperatures, the char does not undergo complete carbonization due to the less release of volatiles; hence the lowest yield of bio-oil and biogas was observed at 300 °C. The decline in biochar yield with elevating pyrolysis temperature is in accordance with previously reported studies (Al Afif et al., 2020; Wang et al., 2020b).

4.2.2 Proximate Analysis

Table 1 provides the proximate analysis results of the feedstock and the prepared biochars. The results show that the quantity of moisture content and volatile matter in the samples reduced, while the ash content increased as the pyrolysis temperature raised. The decrease in the volatile matter is ascribed to the formation of ash matter because the left volatile matter in biochar condensed and the continuous loss of organic matter in the biomass (Shakya and Agarwal, 2019). The ash content increased from 10.664% to 15.2% as pyrolysis temperature increased due to mineral compounds' formation or condensation (Usman et al., 2015). The fixed carbon content increased (19.39% to 34.31%) as the pyrolysis temperature was raised (300°C to 500°C) because the release of volatiles led to a more stable carbon structure. Our results are consistent with previous studies (Chandra and Bhattacharya, 2019; Shakya and Agarwal, 2019; Usman et al., 2015; Yin et al., 2013), which conducted proximate analysis of different biomasses, including cotton stalk, with varying pyrolysis temperatures.

595 **Table 1.** Yield of pyrolysis products and variation in surface properties of produced biochar at
596 distinct pyrolysis temperatures.

Characteristics	Feedstock (CS)	CSB300	CSB400	CSB500
Pyrolysis products yield				
Biochar Yield (%)	-	42	37	30
Bio-oil Yield (%)	-	22	25	28
Biogas Yield	-	36	38	42
Proximate analysis				
Moisture (%)	7.509	4.189	3.645	1.753
VM (%)	74.630	65.760	58.750	48.730
Ash (%)	6.108	10.664	12.699	15.2
FC	11.753	19.388	24.906	34.317
pH and pH_{zpc}				
pH	6.3	6.53	6.67	6.83
Point of Zero Charge (pH_{zpc})	-	7.65	7.7	7.8
Ultimate analysis and molar ratios				
C (%)	46.325	54.413	62.413	69.363
N (%)	1.095	1.350	1.453	1.323
H (%)	5.67	4.163	3.128	2.453
O (%)	40.802	29.411	20.309	11.662
O/C	0.6612	0.4057	0.2642	0.1426
H/C	1.458	0.912	0.597	0.421
(O+N)/C	0.6815	0.427	0.2642	0.1426
BET surface area analysis				
Pore volume (cm^3/g)	-	0.005007	0.03931	0.003207
Pore diameter (nm)	-	4.542	3.3	5.438
Surface area (m^2/g)	-	3.879	32.35	1.922

597

598 **4.2.3 Ultimate analysis**

599 Table 1 indicates the elemental composition of the feedstock and the prepared CSBs.
600 The carbon matter in the CSBs was considerably higher than the feedstock due to the faster
601 and improved carbonization (Chen et al., 2012). CSB400 and CSB500 were class 1

(C>60%) biochars as categorized by the International Biochar Initiative (IBI) (Shakya and Agarwal, 2019). An increase in pyrolysis led to an increase in the biochar's carbon content (46.32% to 69.36%) while the oxygen (40.80% to 11.66%) and hydrogen content (5.67% to 2.45%) declined, which can ascribe to the breakdown of organic components in biomass (Demirbas, 2004). Molar ratios were calculated, providing information regarding the aromaticity and polarity of the materials. The decline in H/C, O/C, (O+N)/C ratios suggests increasing hydrophobicity, prominent aromaticity, and weakening polarity of the produced biochars (Choi and Kan, 2019; Liu et al., 2018). H/C, O/C, and O+N/C ratios decreased due to the decrease in the hydrogen and oxygen content. The decrease in hydrogen and oxygen content is due to the loss of volatiles in the form of CH_4, CO_2, H_2, and CO gases (Xiao et al., 2016). The FTIR analysis (Fig. 6) supported these results as the peaks of OFGs such as –OH (3414 cm^{-1}) and COOH (1620 cm^{-1}) decreased, confirming declining biochar surface polarity. While the bands at ~1430 cm^{-1} (C=C) and 874 cm^{-1} (C-H stretching) intensified as pyrolysis temperature increased, suggesting improving aromaticity. Our results are in accordance with past studies on cotton stalk biochar (Al Afif et al., 2020; Gao et al., 2021; Liu et al., 2018; Makavana et al., 2020).

4.2.4 pH and pHpzc

The solution pH was also monitored by immersing synthesized biochar materials in DI water, with results indicating decreasing trend as CSB500>CSB400>CSB300 (Table 1). Such observation may be attributed to the more significant development of acidic groups such as carboxylic and hydroxyl at lower pyrolysis temperatures, decreasing the solution pH (Kim et al., 2011; Wang et al., 2020b; Zhou et al., 2016). Similarly, the pH_{pzc} of the synthesized biochars showed a decreasing trend as CSB500>CSB400>CSB300 (Fig. 3 and Table 1), which may be attributable to the development of aromatic structures and the loss of acidic functional groups at high temperature (Arabi et al., 2021; Shen et al., 2012).

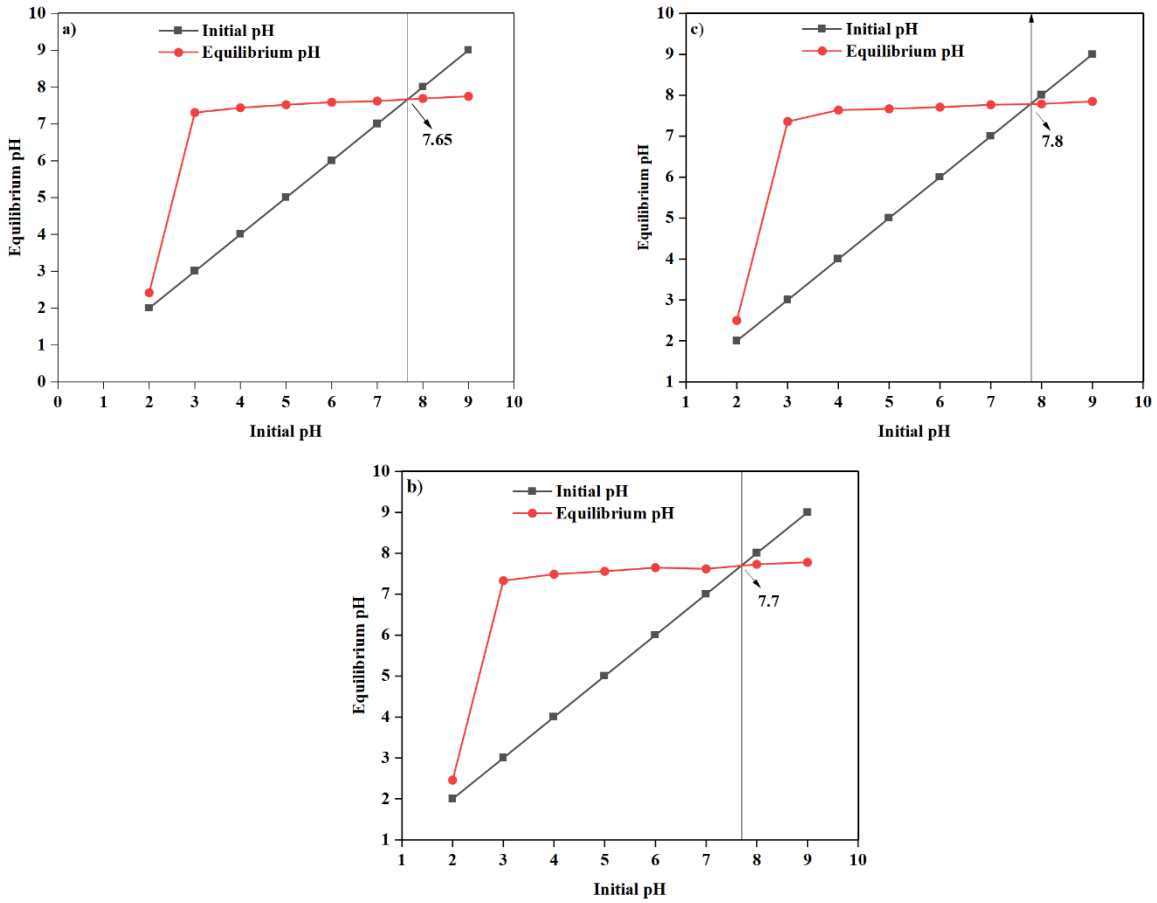

Figure 3. Point of Zero Charge of produced biochars a) CSB300 b) CSB400 c) CSB500

627

628 **4.2.5 Thermogravimetric Analysis**

629 Thermogravimetric analysis was performed to examine temperatures' effect on the
630 weight loss of biomass. The weight of the biomass gradually decreased with increasing
631 temperature (Fig. 4). At 800 °C, the total weight loss obtained was 98% of the total biomass
632 weight, which can be ascribed to dehydration and loss of volatiles. At 110 °C, the weight
633 loss indicates the moisture content (8.82%). The loss of 2% of the total weight between
634 110 °C and 191 °C is assigned to the residue molecules, volatiles, and bound water (Li et
635 al., 2017). The thermal degradation of hemicellulose caused a weight loss of 15.9%
636 between 191 °C and 280 °C. Similarly, the thermal breakdown of cellulose is responsible
637 for the weight loss of 41.52% between 281 °C and 380 °C (Lee et al., 2013). A weight loss
638 of 21.55% occurred due to the breakdown of lignin, which is maximum between 350 °C
639 and 450 °C (Nassar and MacKay, 1984).

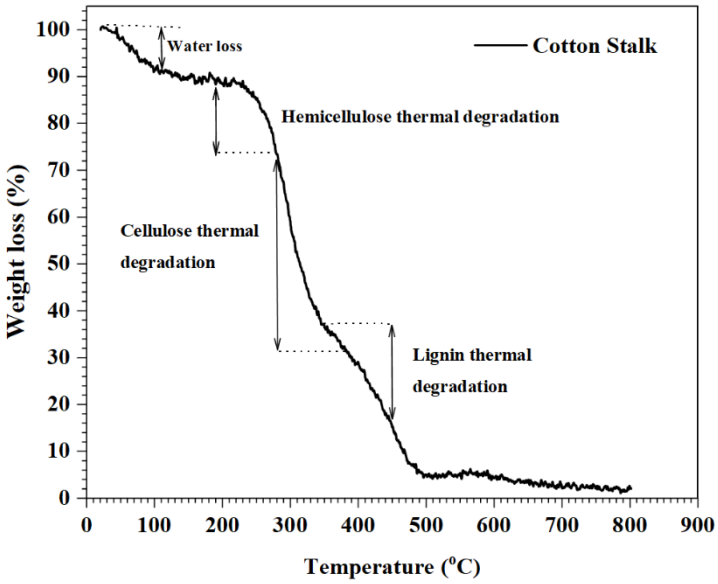

Figure 4. TGA analysis of feedstock (cotton stalk)

4.2.6 SEM-EDS

SEM images depicted the variation in surface morphology of CSBs with varying pyrolysis temperatures (Fig. 5). As shown in Fig. 5 (a, b), CSB300 and CSB400 surfaces are rough and porous (honeycomb-like structures). The increasing loss of volatile matter with increasing pyrolysis temperature resulted in increasing porosity, consequently enhancing the adsorbent's surface area (BET analysis) (Tariq et al., 2020). The CSB500 had a rough surface, but the pore structure collapsed due to high pyrolysis temperature, which is also supported by the BET analysis, as CSB500 had the lowest surface (Table 1) (Gao et al., 2021). ARCSB500 SEM image showed that the pores were visibly blocked, possibly due to the Cr uptake (Fig. 5d; Table 5). The EDS analysis showed no Cr uptake on the raw biochar surface, but the Cr uptake by CSB500 was confirmed as it was detected on the ARCSB500 surface. The EDS analysis revealed that the biochars' main chemical components were C, O, Mg, Sil, Na, K, and Ca, with a trace amount of Ne also detected (Table 2-4).

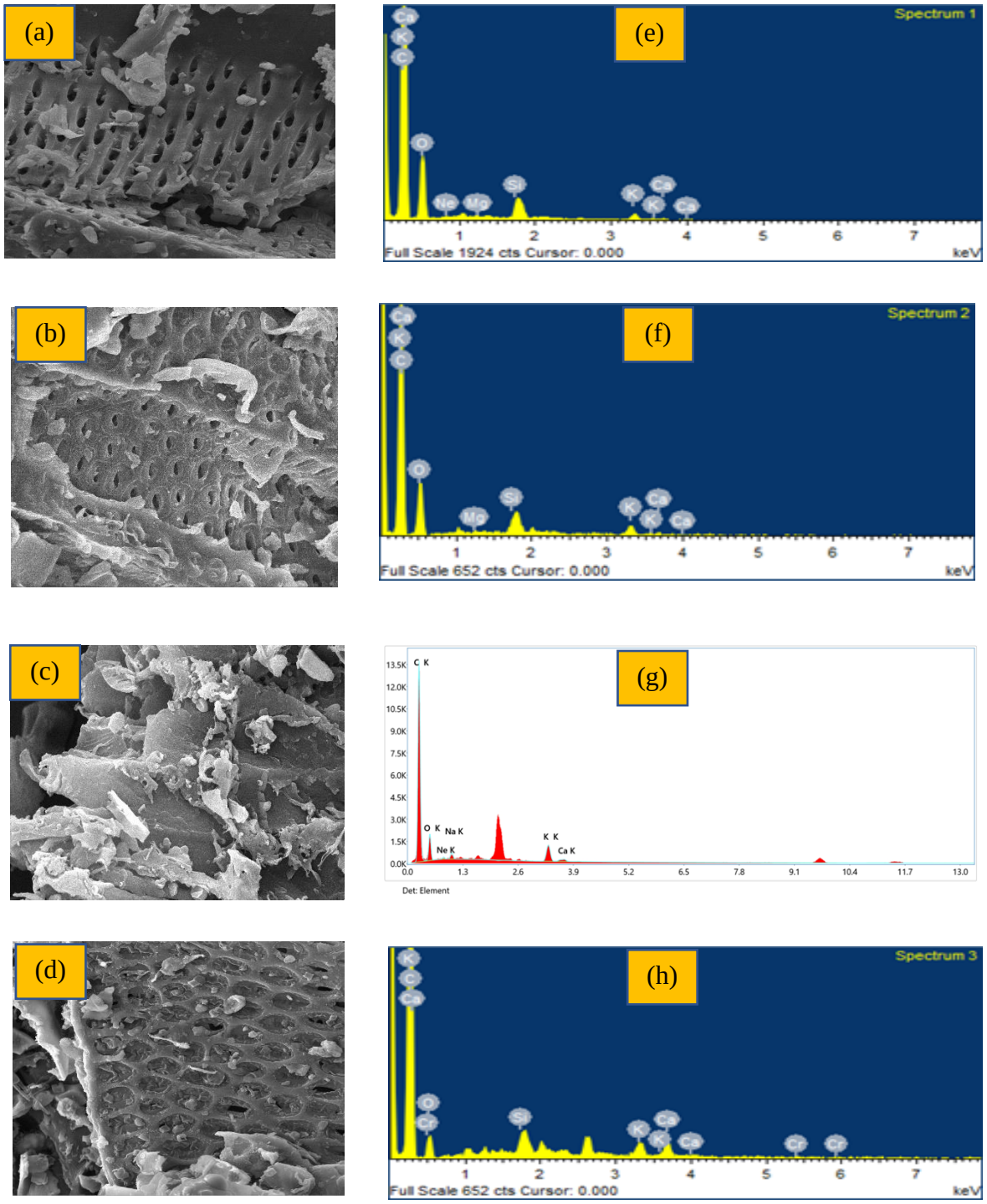

Figure 5. SEM-EDS images of biochar of (a,e) CSB300 (b,f) CSB400 (c,g) CSB500 and (d,h) ARCSB500

682

683 **Table 2.** CSB300 elemental composition

Element	Weight (%)	Atomic (%)
C	76.17	82.12
O	20.62	16.69
Ne	0.17	0.11
Mg	0.13	0.07
Si	0.35	0.16
K	2.12	0.70
Ca	0.44	0.14

684

685 **Table 3.** CSB400 elemental composition

Element	Weight (%)	Atomic (%)
C	72.2	79.50
O	22.55	18.64
Mg	0.38	0.21
Si	0.07	0.03
K	4.13	1.40
Ca	0.68	0.22

686

687 **Table 4.** CSB500 elemental composition

Element	Weight (%)	Atomic (%)
C	58.8	68.5
O	30.7	26.8
Ne	0.8	0.6
Na	2.7	1.7
K	6.0	2.1
Ca	0.9	0.3

688

689 **Table 5.** ARCSB500 elemental composition

Element	Weight (%)	Atomic (%)
C	85.71	89.97
O	11.61	9.15
Si	0.30	0.13
K	1.08	0.35
Ca	1.14	0.36
Cr	0.15	0.04

690

4.2.7 BET analysis

The BET surface area of CSB300 was 3.879 m^2/g, pore volume of 0.005007 cm^3/g, and pore diameter of 4.542 nm. In comparison, CSB400 had the highest surface area (32.35 m^2/g) and pore volume (0.03931 cm^3/g), possibly due to the loss of volatile matter as pyrolysis temperature raised, leading to a more porous structure (Angın, 2013). However, CSB500 had the lowest surface area (1.922 m^2/g), possibly because at a higher temperature, the structural deformation or collapse of the pores structure could occur (Li et al., 2017). This trend was observed in other studies where after a certain point, an increase in pyrolysis temperature decreased the adsorbent's surface area (Gao et al., 2021; Li et al., 2017; Shakya and Agarwal, 2019). Interestingly, the CSB500 had better Cr (VI) adsorption capacity compared to CSB300 and CSB400. This result implies that the surface area of adsorbents is not the leading parameter in determining Cr (VI) adsorption performance of biochar. This is well supported by literature where mainly chemical processes are the controlling factors in Cr (VI) adsorption (Gao et al., 2021; Shakya and Agarwal, 2019; Zhang et al., 2018b).

4.2.8 FTIR analysis

The FTIR analysis indicates the bonding features of the pristine and Cr (VI) loaded CSB300, CSB400, and CSB500 biochars (Fig. 6). Before adsorption, the broad trough around 3414 cm^{-1} indicates hydroxyl groups (-OH bond) (Yusuff et al., 2022). The peaks around 2926 cm^{-1} and 2846 cm^{-1} indicate the C-H stretching, long-chain asymmetric aliphatic components of the $-CH_2$ and $-CH_3$ groups, respectively (Ma et al., 2019a); the peak around ~1620 cm^{-1} correspond to carboxylic acid COOH (Rafique et al., 2021; Sikder et al., 2013). The peaks around 1430 cm^{-1} were generated by aromatic C=C rings stretching vibrations (Wang et al., 2019). The hydroxyl bending vibration and carbon-oxygen bond (COC) were also detected as the peaks around 1315 cm^{-1} and 1110 cm^{-1} indicate their presence (Dong et al., 2011; Wang et al., 2020a). The band at ~874 cm^{-1} confirms the aromatic C-H bending vibration (Wang et al., 2014). The FTIR analysis of ARCSB300, ARCSB400, and ARCSB500 showed that the intensity of the peaks around 3417 cm^{-1}, 2926 cm^{-1}, 2846 cm^{-1},1620 cm^{-1}, and 874 cm^{-1} reduced. These results suggested the contribution of the aforementioned bonds in the Cr (VI) sorption process.

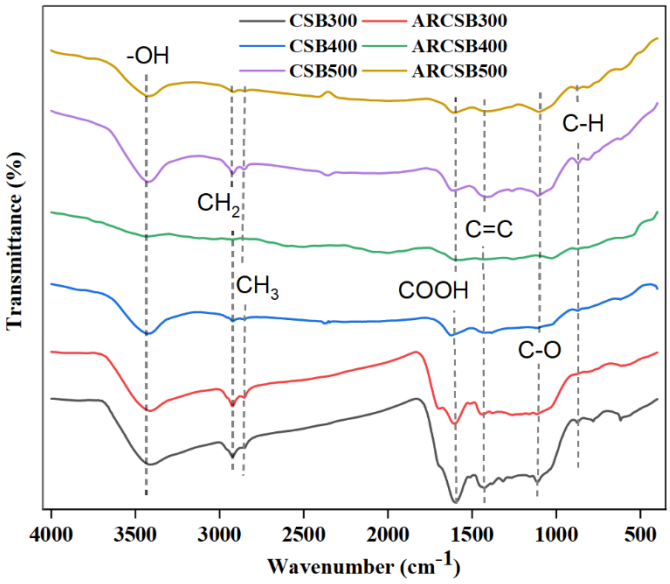

Figure 6. FTIR analysis of CSB300, CSB400, and CSB500 before and after Cr (VI) removal.

4.2.9 X-ray diffraction analysis (XRD)

As evident in XRD patterns of CSB300, CSB400, and CSB500, the peaks at 2θ = 28.3°, 40.3°, 50.2°, 66.1° and 73.5° correspond to the (2 0 0), (2 2 0), (2 2 2), (4 2 0), and (4 2 2) crystalline planes, respectively, indicating KCl presence according to the standard card (JCPDS no. 41-1476) (Wang et al., 2017). The fringe pattern at 2θ =22.2° and 43.0° correspond to the (1 0 0) and (1 1 1) planes, respectively, which agreed to the database of SiO_2 (amorphous structure) standard card (JCPDS-ICDD) (Tański et al., 2017).

According to the Debye–Scherrer equation (Eq. 18), the average crystallite size of KCl and SiO_2 phases for CSB300, CSB400, and CSB500 equal 7.9 nm and 18.1 nm, 8.3 nm and 19.4 nm, and 9.5 nm and 21.9 nm, respectively. The Debye–Scherrer equation is as follows:

$$D = K\lambda/\beta\cos(\theta) \qquad \text{(Eq. 18)}$$

where D is the diameter of the crystallite size, K is the shape factor (the typical value is 0.9), λ is the wavelength of the incident beam, and β is the broadening of the diffraction line measured in radians at half of its maximum intensity (FWHM), and θ is the Bragg's angle (Hajizadeh et al., 2022).

The increase in crystallite size of the phases at higher temperatures may be ascribed to the thermally promoted crystallite growth. For ArCSB300, ArCSB400, and ArCSB500,

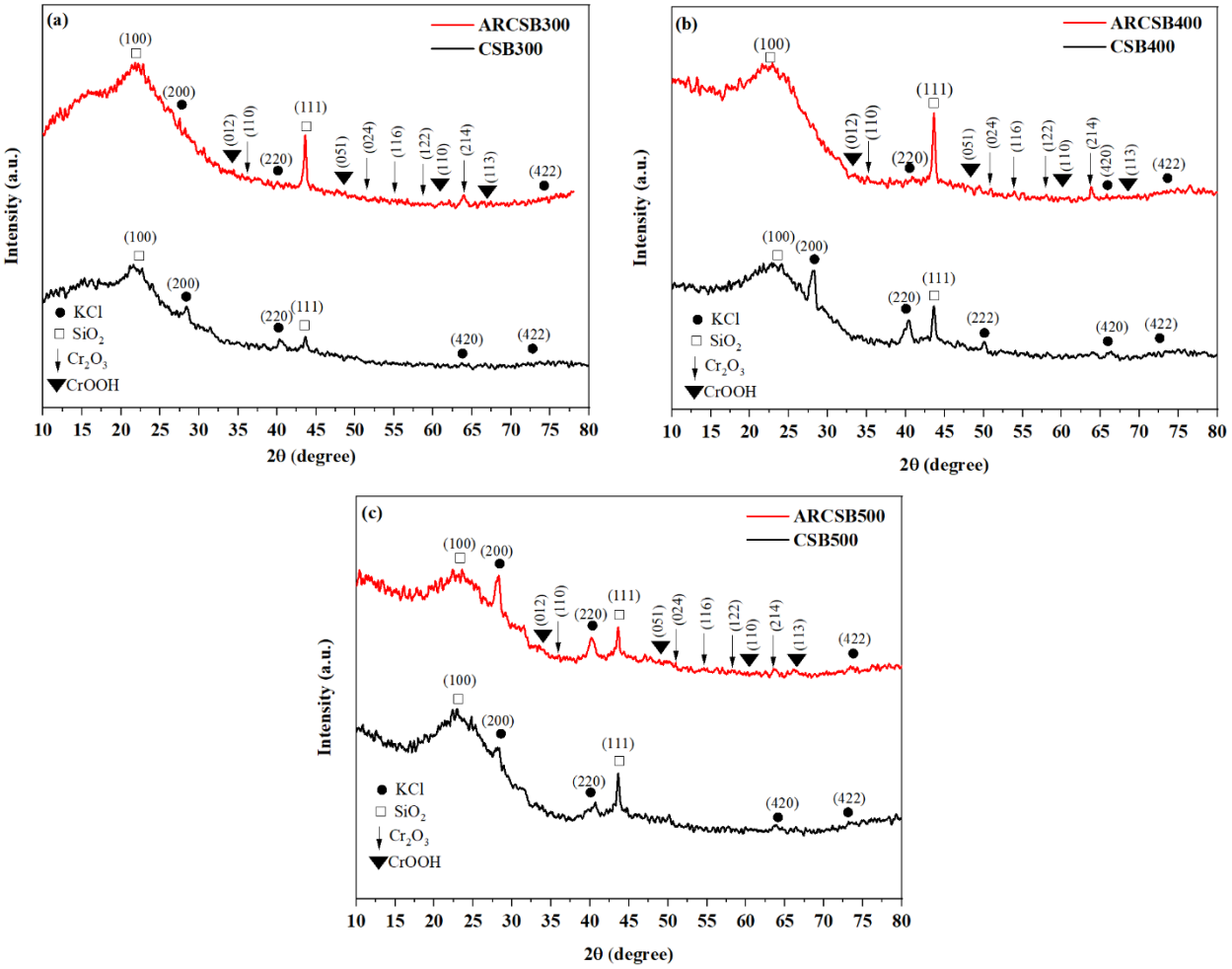

Figure 7. XRD pattern of produced biochar before and after chromium sorption a) CSB300 and ARCSB300 b) CSB400 and ARCSB400 c) CSB500 and ARCSB500.

the average crystallite size of KCl and SiO_2 phases equals 8.0 nm and 20.8 nm, 8.5 nm and 22.5 nm, and 9.2 nm and 30.2 nm, respectively. The crystallite size of KCl and SiO_2 phases after Cr (VI) adsorption, did not change significantly, indicating that the Cr (VI) doping onto the crystalline structures of KCl and SiO_2 phases cannot be considered as major mechanism responsible for Cr (VI) adsorption process.

According to the XRD patterns of the loaded Cr (VI) samples, the diffraction peaks at $2\theta = 36.4°$, 50.1°, 54.8°, and 57.7° are assigned to the (1 1 0), (0 2 4), (1 1 6), and (1 2 2) crystalline planes, respectively, which matches with the Cr_2O_3 standard card (JCPDS no.

38-1479). In addition, the diffraction peaks at 2θ = 34.9°, 48.6°, 59.9°, and 65.8° are assigned to the (0 1 2), (0 5 1), (1 1 0), and (1 1 3) crystalline planes, respectively, which matches with the CrOOH standard card (JCPDS no. 70-0621). The formation of Cr_2O_3 and CrOOH shows the reduction of Cr (VI) ions to Cr (III) species. Therefore, governing mechanisms responsible for Cr (VI) adsorption on the biochar may be surface interactions, Cr (VI) reduction to Cr (III) followed by surface adsorption (Li et al., 2013; Tong et al., 2011).

Noteworthy, the intensity of some peaks of the biochar decreased after the adsorption process (Fig. 7). Such phenomenon may be related to the existence of some inorganic component (e.g., KCl) in an aqueous solution during the sorption process. In addition, by comparing the XRD peak intensities of the loaded samples, the peak intensities of the Cr_2O_3 phase in ArCSB300 and ArCSB400 are more than those available in the pattern of ArCSB500. In comparison, the peak intensities of CrOOH in ArCSB500 are higher, showing that the Cr (VI) ions tend to precipitate on CSB300 and CSB400 as Cr_2O_3, while at CSB500, the ions tend to precipitate as CrOOH crystalline phase.

4.3 Adsorption Performance of biochars

4.3.1 Effect of adsorbent dosage (Selection of adsorbent)

Selecting the optimal adsorbent dose is crucial in determining adsorbent effectiveness (Zhang et al., 2017). The dosage experiments were performed using the produced biochars, i.e., CSB300, CSB400, and CSB500. As shown in Fig. 8, equilibrium was reached at 3 g/L. At equilibrium, for CSB300, CSB400, and CSB500 the removal potential and sorption affinity were 75%, 85%, 99% and 4.98, 5.65, and 6.54 mg/g, respectively. The sorption affinity improved because the available surface area and active sorption sites increased. Although, this trend was not followed strictly for adsorbent dosage greater than 3 g/L because the available sites were saturated with Cr (VI) ions, and negligible solute was left

in the solution (Al-Homaidan et al., 2018; Tariq et al., 2020). Hence, CSB500 with an equilibrium dosage (3g/L) was selected for subsequent sorption experiments.

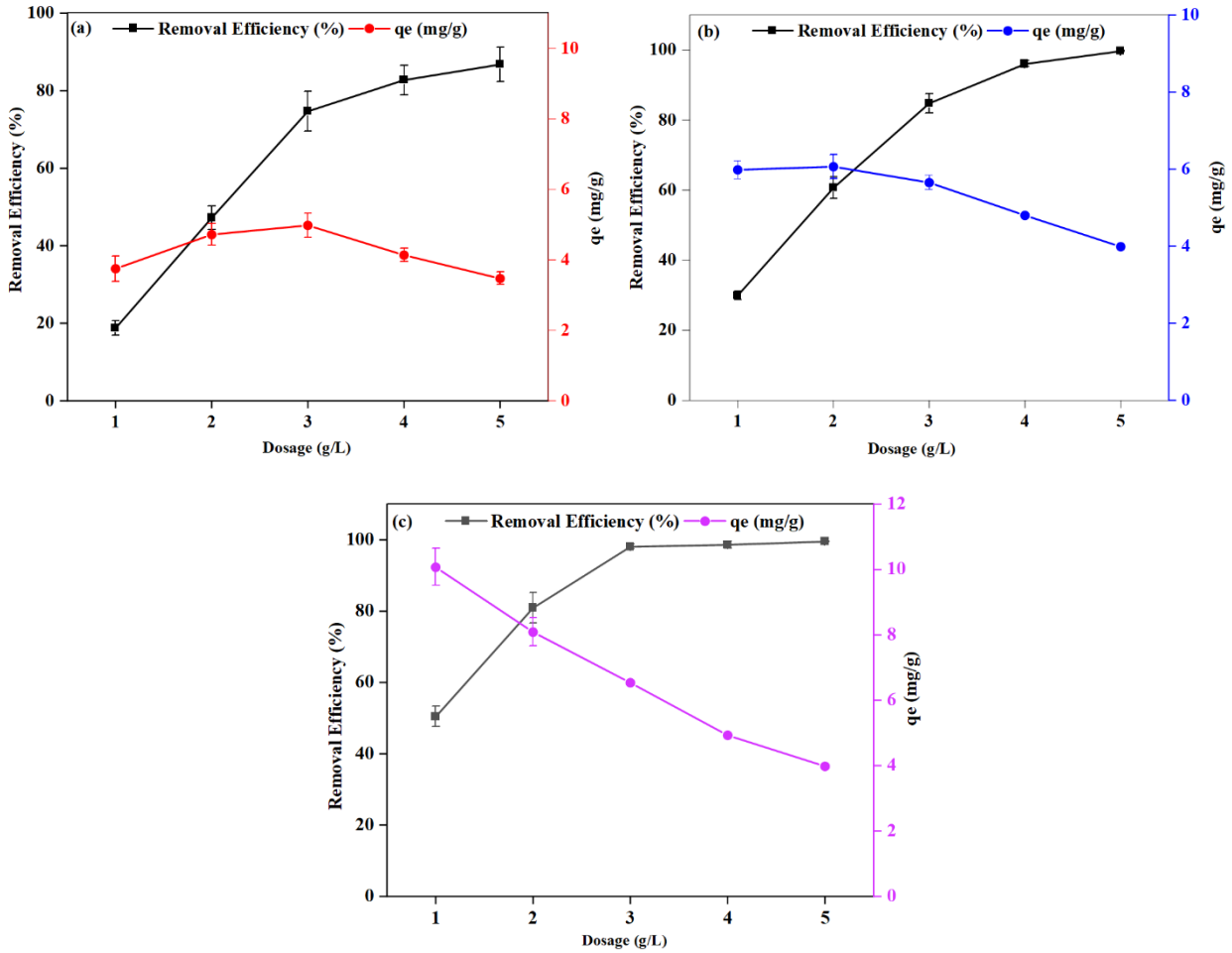

Figure 8. Effect of biochar dosage on Cr (VI) removal efficiency a) CSB300 b) CSB400 c) CSB500

4.3.2 Batch experiments for selected adsorbent

4.3.2.1 Contact time and adsorption kinetics

Fig. 9 displays that the CSB500 sorption rate during the first half is rapid and becomes steady as the contact time increases. The adsorption reaction reached equilibrium at 120 mins (97% removal, 6.46mg/g adsorption capacity). During the first hour, approximately 87% of the Cr (VI) was removed, probably due to many adsorption sites accessible to Cr (VI) attachment before reaching equilibrium (Choudhary and Paul, 2018; Liang et al., 2020). Also, with progressing time, the surface gets saturated with Cr (VI) ions; these anions cause electrostatic repulsion with each other, consequently slowing down the

adsorption process as it approaches equilibrium (Cherdchoo et al., 2019). A contact time of 2 hours was found to be optimal and used for used subsequent experiments.

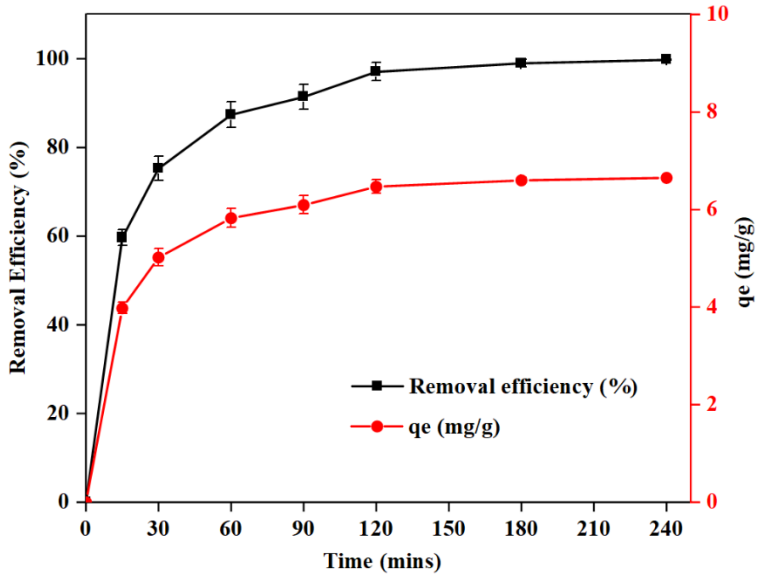

Figure 9. Influence of contact time on CSB500 Cr (VI) removal and sorption affinity.

PSO and PFO kinetic models were applied to the CSB500 adsorption data to understand its kinetic behavior (Fig. 10). The results in Table 6 show that although both the models show an excellent correlation, comparatively, the PSO model fits better (R^2>0.999 vs. R^2>0.998) (Table 6). These results suggest that physisorption and chemisorption were involved in Cr (VI) elimination, but the sorption process was more inclined toward chemisorption. The PSO model assumes that two factors control the adsorption rate, i.e., available active surface sites and adsorbate concentration. This assumption conforms with the experimental results as initially, the adsorption capacity increases rapidly and slows down gradually during the later stages.

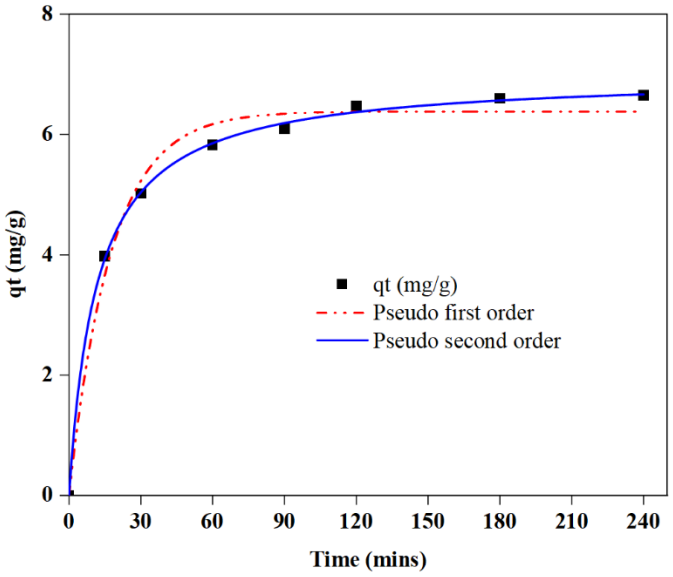

Figure 10. Kinetic model plot.

Table 6. Kinetic parameters for Cr (VI) adsorption onto CSB500

Adsorbent		Pseudo first order			Pseudo Second order		
	q_{exp} (mg/g)	$q_{e,\ cal}$ (mg/g)	K_1 (min^{-1})	R^2	$q_{e,\ cal}$ (mg/g)	K_2 ($g.mg^{-1}.min^{-1}$)	R^2
CSB500	6.46	6.381	0.05703	0.9851	6.9897	0.0123	0.99924

q_{exp} = experimental, $q_{e,\ cal}$ = calculated

4.3.2.2 Effect of solution pH on adsorption performance

The pH of a solution significantly influences the efficiency and effectiveness of biochar sorbents. Batch experiments showed that pH 2 was optimal for Cr (VI) sorption, where the highest removal occurred (99%) (Fig. 11). The removal efficiency of the sorbent drastically drops to 38% at pH 3, from pH 4 to 9; though the removal capacity declines steadily from 20% to 7%, the adsorbent effectiveness is compromised severely. An abundance of the literature also suggests that for Cr (VI) removal, pH=2 is optimal (Dong et al., 2011; Guo et al., 2020; Shakya and Agarwal, 2019). In the acidic pH range (<6.3), Cr (VI) exists mainly in $HCrO_4^-$ and $Cr_2O_7^{-2}$ forms and in the CrO_4^{-2} form in the higher pH (>6.3). In the lower pH, as H^+ ions are abundant, the CrO_4^{-2} form gains a proton to form $HCrO_4^-$, and in the pH below 1, the CrO_4^{-2} ion becomes H_2CrO_4 compound by gaining two protons (Fig.

12) (Mohan et al., 2011; Zhitkovich, 2011). $HCrO_4^-$ requires one exchangeable site, while at higher pH, chromium exists as CrO_4^{-2}, which requires two exchangeable sites, thus making the adsorption process more challenging (Kuppusamy et al., 2016). At lower pH, the abundant H^+ ions cause the surface functional groups to be protonated, therefore presenting the positive surface charge. Thus, the electrostatic interaction between Cr (VI) ions and the positively charged surface plays a role in Cr (VI) sorption (Shakya and Agarwal, 2019). Also, at $pH<pH_{zpc}$, the H^+ overcomes the OH^- ions, improving adsorption capability at lower pH (Tariq et al., 2020). At pH 3 and above, the significant drop in removal capacity may be attributed to increasing OH^- ions in the solution. The negatively charged hydroxide ions compete with Cr (VI) for active sorption sites, and for the positively charged surface sites and may also cause electrostatic repulsion (Ma et al., 2019a). Hence, the optimal pH (2) was considered for subsequent sorption experiments.

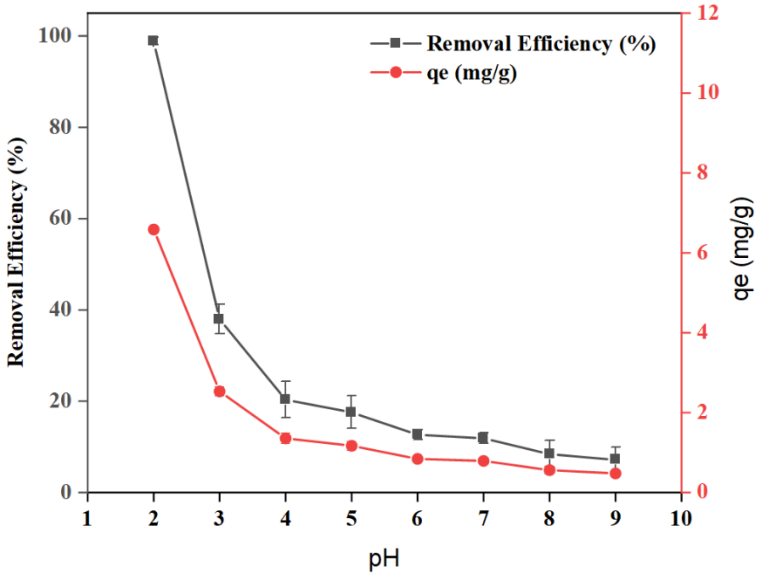

Figure 11. Influence of initial pH on Cr (VI) removal and sorption affinity by CSB500.

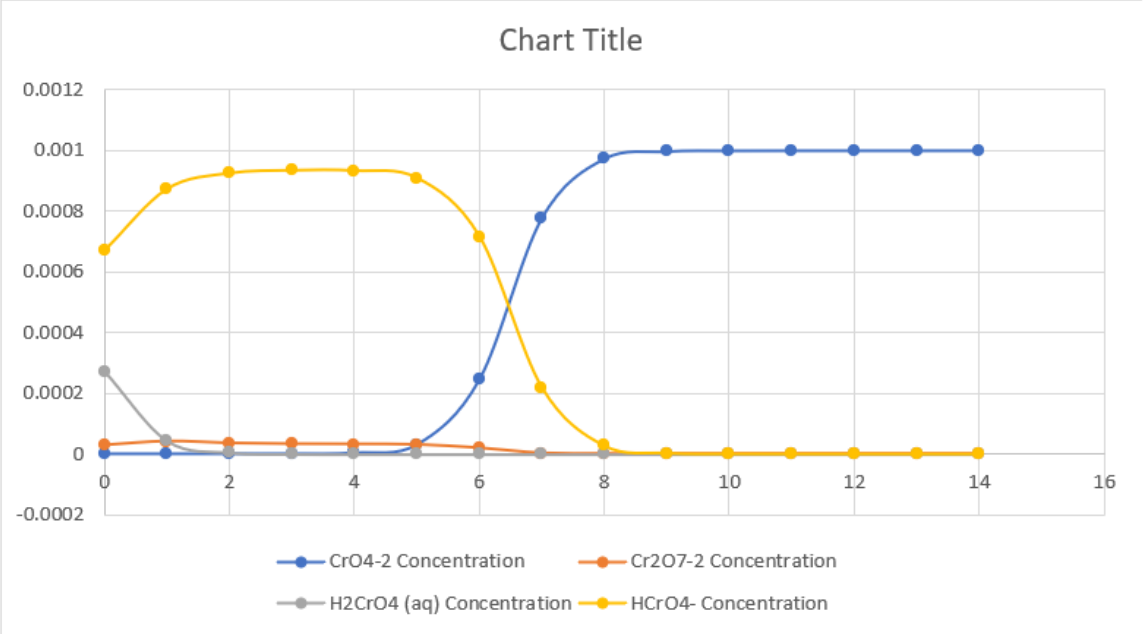

Figure 12. Chromium Speciation

4.3.2.3 Influence of initial Cr (VI) concentration and temperature

The experimental data shows that CSB500 removal efficiency was positively affected by rising atmospheric temperature, but the presence of a greater concentration of Cr (VI) ions in the solution had a negative impact on it (Fig. 13). When the Cr (VI) concentration in the suspension is low, the available sites on the biochar surface are comparatively more for adsorption. The available sites are comparatively less when the Cr (VI) concentration in the solution grows, and electrostatic repulsion strengthens, resulting in weak adsorption

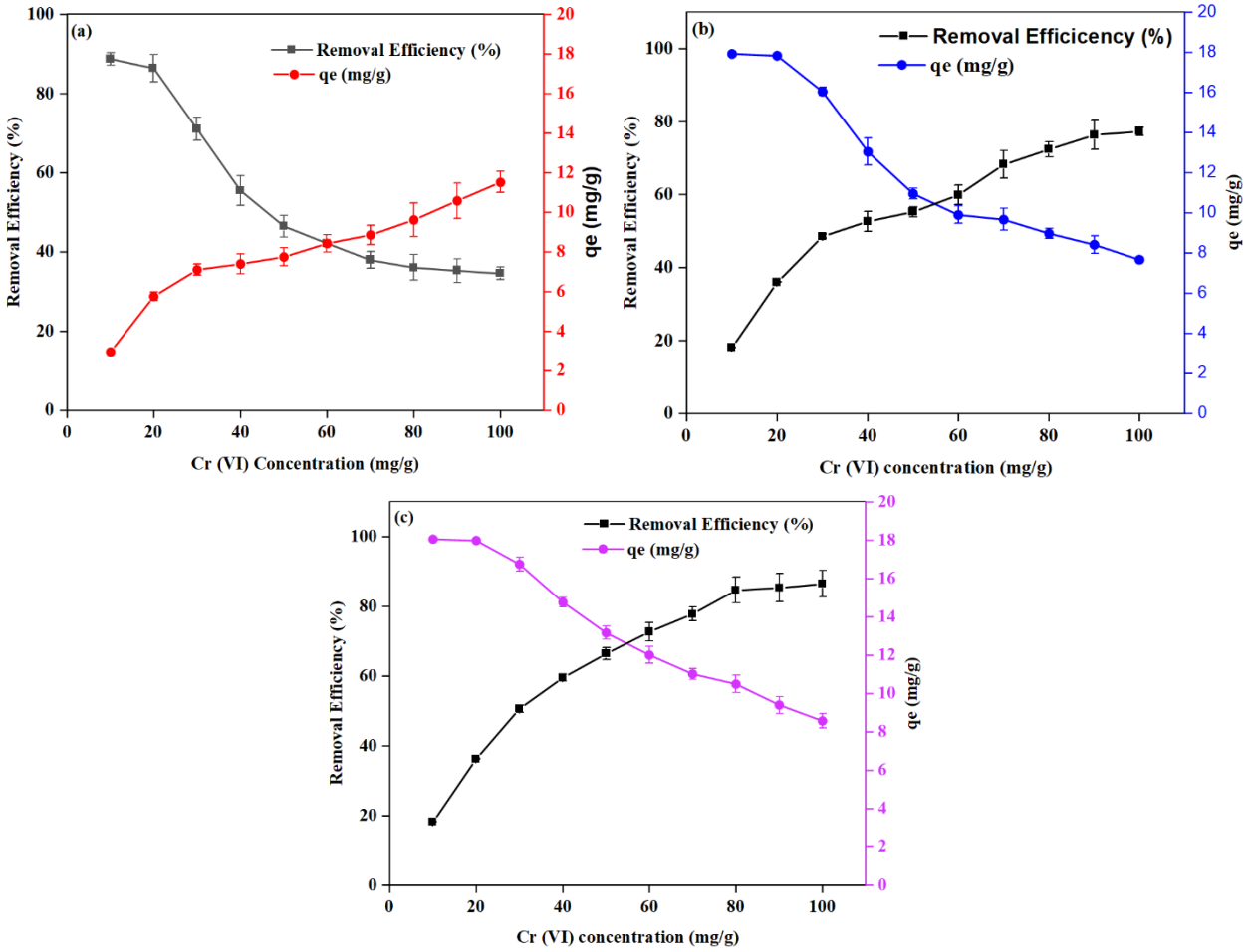

Figure 13. Impact of initial Cr (VI) concentration on sorption performance of CSB500 at various temperature conditions a) 15°C b) 25°C c) 35°C.

performance (Imran et al., 2020; Tariq et al., 2020). At 25 °C, the experimental q_{max} (mg/g) of CSB500 was calculated to be 14.045 mg/g and C_e (mg/L) of 57.86 mg/L.

Fig. 14 presents the sorption isotherms, and Table 7 indicates the corresponding parameter values. The results indicated that the Freundlich model with a higher correlation coefficient ($R^2 > 0.967$) fitted better with the experimental data than the Langmuir model ($R^2 > 0.856$). This suggests that the adsorbent's surface is heterogenous, its active sites have a varied affinity for the adsorbate, and their interaction is in the form of multilayers rather than monolayers. Adsorption isotherm results are consistent with our FTIR results (Fig. 6), where functional groups (-OH, C=C, COOH, $-CH_2$, $-CH_3$) on the CSBs surface played a critical role in Cr (VI) sorption. Also, the 1/nF value for the CSB500 was less than 1, which signifies favorable conditions for the Cr (VI) sorption onto CSB500. The sorption affinity of the CSB500 increased (11.51 mg/g to 15.71 mg/g) with increasing temperature

(15°C to 35°C), suggesting the endothermic nature of the sorption process (Song et al., 2015).

Table 7. Adsorption isotherm parameters for Cr (VI) sorption onto CSB500

	Langmuir Parameters			Freundlich Parameters		
Temp (°C)	Q_{max} (mg/g)	K_L (L/mg)	R^2	K_f ($mg^{1-1/n}L^{1/n}$ g^{-1})	1/nF	R^2
15	9.560	0.317	0.904	3.483	0.252	0.895
25	11.930	2.429	0.879	6.388	0.184	0.904
35	13.950	3.830	0.863	7.661	0.192	0.967

Table 8. Adsorption thermodynamic parameters

Temp (°C)	K_L (L/mg)	ΔG° (kJ/mol)	ΔH° (kJ/mol)	ΔS° (J/mol-K)
15	0.345	-13.989	81.301	0.333
25	2.371	-19.253		
35	3.070	-20.561		

The mathematical models for thermodynamic parameters are shown in Section 3.8 (Eq 16 and 17). Table 8 indicates the thermodynamic parameters, where the ΔG° values were all negative, indicating a spontaneous adsorption process (Guo et al., 2020). The absolute ΔG° (change in free energy) values increased with increasing reaction

temperature, thus enhancing the spontaneity of the process. The positive ΔH° value confirms the endothermic nature of the sorption process. Also, the ΔH° value of more than 40 kJ/mol suggests chemisorption as the dominant process, which is supported by the results of kinetic models as the experimental data was better fitted with the PSO model (Gupta et al., 2013). Additionally, the positive ΔS° value implies an increase in randomness during the sorption of Cr (VI) onto CSB500 (Hu et al., 2011).

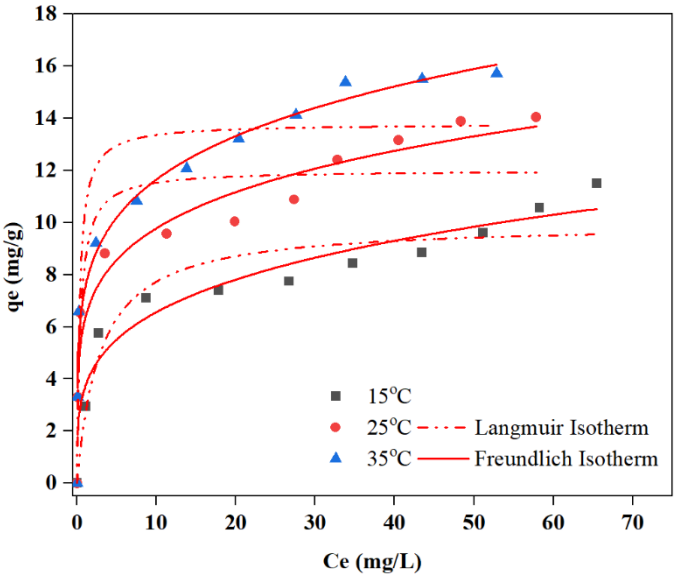

Figure 14. Adsorption Isotherm models plot.

4.3.2.4 Interfering ions effect

Since wastewater contains multiple ions that can influence the biochar adsorption capacity, Suspensions with 100 mg/L of phosphate, sulphate, chloride, and nitrate along with 20 mg/L Cr (VI) were prepared and experiments were conducted under optimal conditions. Fig. 15 shows that these selected anions had an insignificant effect on the Cr (VI) removal capacity. The change was less than 3%; hence, we can conclude that these selected foreign ions did not compromise the CSB500 adsorption capacity. Further work needs to be done on the ions present in industrial wastewater, especially in industries where Cr (VI) discharge is more prominent such as tannery, electroplating, smelting, and mining.

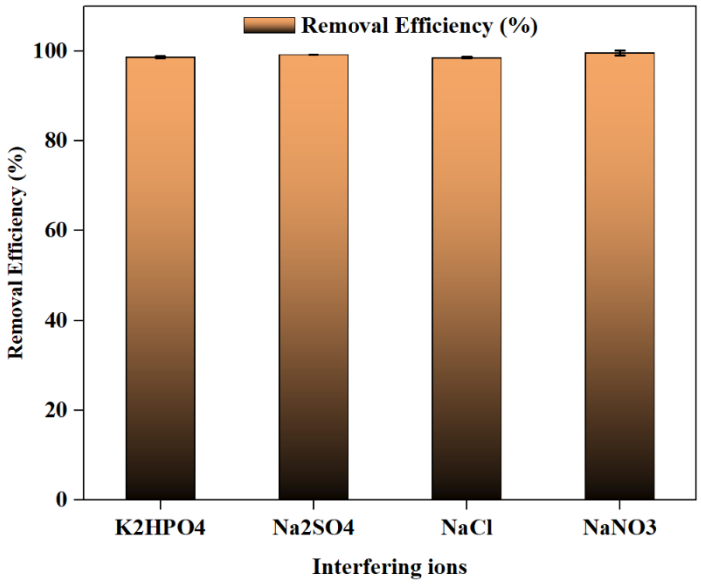

Figure 15. Interfering ions effect on CSB500 Cr (VI) removal efficiency and adsorption capacity.

4.3.2.5 Regeneration and reusability

A reusability study is essential in determining an adsorbent's effective life span. In this study, the reusability of CSB500 was tested for three adsorption/desorption cycles. As shown in Fig. 16, sorption affinity declined with each successive cycle (from 99% to 27%). This declining trend could be caused by weakening functional groups or partial blocking of pores on sorbent surfaces (Shakya and Agarwal, 2019). It can be concluded from experimental results that the current CSB500 still holds some potential in terms of its reusability and stability. However, other improvement techniques like surface modification could be implied to augment the reusability potential of the produced biochar material (Mdlovu et al., 2020; Wang et al., 2020a; Zhong et al., 2019).

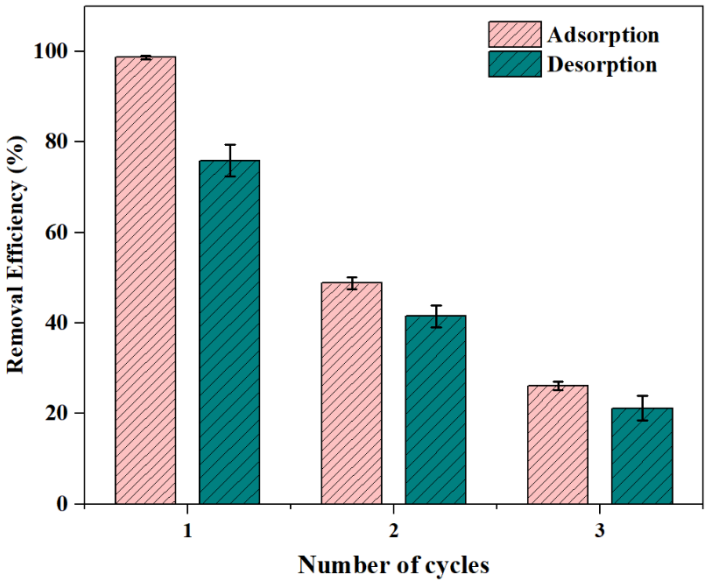

894

895 **Figure 16.** Reusability potential of CSB500 biochar.

896 ## 4.4 Removal mechanism

897 To understand the mechanism behind the removal of Cr (VI) species and to determine
898 why biochar prepared at a certain temperature from the same feedstock performed better
899 than the others, adsorption experiments and analytical procedures were employed. The
900 adsorption studies showed that Cr (VI) removal in acidic conditions was favorable, whereas
901 a pH of 2 was optimal. The high removal at lower pH can be ascribed to the fact that OFGs
902 such as hydroxyl and carboxyl groups are protonated ($-OH_2^+$, $COOH_2^+$) at lower pH where
903 H^+ ions are in abundance. The protonation of such functional groups enhances the
904 electrostatic attraction between the CSB protonated surface and Cr anions. Also, at pH <3,
905 Cr (VI) dominant form is $HCrO_4^-$ which requires only one exchangeable site, while at
906 pH>3, $Cr_2O_7^{-2}$ and CrO_4^{-2} are predominantly found, requiring two exchangeable sites.
907 Therefore, the CSB500 performed better at lower pH. The kinetics and adsorption studies
908 supported the electrostatic phenomenon as the PSO model and Freundlich isotherm better
909 fitted the experimental data, suggesting chemisorption (covalent interactions and
910 electrostatic attraction) as the dominant process and that the interaction between sorbents'
911 heterogeneous surface and Cr (VI) ions were in a multilayer form.

912 Multiple characterization tools were used to analyze the prepared biochars. SEM
913 analysis showed that the biochars had rough and honeycomb-like porous structures,

914 indicating a potential for Cr (VI) physical adsorption. ARCSB500 showed that the surface
915 after adsorption was visibly blocked, possibly due to the Cr (VI) deposition. The EDS
916 analysis of ARCSB500 confirmed the Cr (VI) uptake (Table 5). The BET analysis (Table
917 1) indicated that the biochar's BET surface area was not the leading factor in determining
918 its Cr (VI) removal efficiency, as CSB500 had the lowest surface area but the highest
919 adsorption capacity. The FTIR analysis was conducted for the raw and Cr (VI) loaded
920 biochars. Fig. 6 shows that after adsorption, the broad peak at 3417 cm^{-1} (-OH bond in
921 hydroxyl groups), the peaks around 2926 cm^{-1} ($-CH_2$), 2846 cm^{-1} ($-CH_3$), 1620 cm^{-1}
922 (COOH), and 1430 cm^{-1} (C=C) intensity reduced suggesting the participation of these
923 reactive groups in Cr (VI) removal. The results agree with other studies suggesting these
924 reactive groups' involvement in Cr (VI) sorption process (Dong et al., 2011; Ma et al.,
925 2019a; Wang et al., 2019; Zhang et al., 2018a; Zhou et al., 2016). The participation of -
926 CH_2, $-CH_3$, COOH, C=C, and C-H functional groups in the CSB500 was more intense than
927 in the other biochars, which might be the reason for improved adsorption results. After Cr
928 (VI) removal, the XRD pattern changed significantly from the raw biochar pattern,
929 showing a decrease in the existing peaks, and some new peaks emerged, which declared
930 the existence of chromium compounds (Cr_2O_3 and CrOOH) on the CSB surface. The
931 presence of these chromium compounds suggests that the Cr (VI) reduced to Cr (III) ions.
932 Although the XRD pattern indicated the existence of KCl and SiO_2 crystal structures, these
933 organic compounds were not involved in Cr (VI) removal as no significant changes in
934 crystalline size were noted. The multiple characterization results suggest that initially, the
935 biochar removed Cr (VI) via electrostatic attraction. Afterwards, OFG's donated electrons
936 to Cr (VI), causing its reduction to Cr (III), followed by complex formation with surface

functional groups. The batch experiments in this study, thus, indicated that the removal of Cr (VI) increased with CSB500 than CSB300 and CSB400, whereas available literature suggests it should be otherwise (Shakya and Agarwal, 2019; Wang et al., 2019; Xu et al., 2022; Zhou et al., 2016). The previous studies have focused more on OFGs role, while in this study, we suggest that other functional groups (-CH_2, -CH_3, C=C. and C-H) and other governing factors may be involved in Cr (VI) removal. To further illustrate the reason behind the high adsorption affinity of CSB500/Cr (VI) reaction, inside shedding into the molecularly fine structure of ARCSB500 is required.

Figure 17. Cr (VI) removal mechanism

CHAPTER 5

5 Conclusions

This study comprehensively investigated the temperature-dependent variation in the surface properties of CSBs and its role in Cr (VI) removal from aqueous environments. For this purpose, we prepared low-cost adsorbents (CSB300, CSB400, and CSB500) at various pyrolysis temperatures and evaluated the produced biochar adsorption performance by conducting batch adsorption experiments. The series of batch adsorption experiments showed that increasing the solution's pH had a negative impact, while increasing pyrolysis temperature positively impacted biochar adsorption performance. Furthermore, CSB500 indicated higher ash content, fixed carbon, pH, and pHpzc. However, the same trend was not followed for moisture content, volatile matter, H/C, and O/C ratios, which decreased. The experimental data fitted well with the Freundlich isotherm and PSO kinetics model, indicating the adsorption process was inclined considerably towards chemisorption. Characterization tools confirmed that the surface area was not an important factor in governing the Cr (VI) removal performance. The Cr (VI) removal mechanism, as suggested by the isotherm and kinetic models and the characterization results, could be attributed to the chemical processes such as electrostatic attraction, followed by Cr (VI) reduction to Cr (III) and complexation between the Cr ions and reactive groups present on CSB surface. The impact of co-existing ions on CSB500 adsorption performance was negligible. The reusability potential of the adsorbent indicated a significant decline in Cr (VI) removal, thus suggesting further improvement in surface characteristics and stability of our produced sorbent before proceeding towards commercialization. Overall, our study suggests the potential of low-cost adsorbent material in this study is effective in removing Cr (VI) from chromium-contaminated streams. However, further studies need to be focused on improving the biochar stability and physicochemical properties to treat Cr (VI) containing wastewater.

6 References

Al-Homaidan, A.A., Al-Qahtani, H.S., Al-Ghanayem, A.A., Ameen, F. and Ibraheem, I.B.M. 2018. Potential use of green algae as a biosorbent for hexavalent chromium removal from aqueous solutions. Saudi Journal of Biological Sciences 25(8), 1733-1738.

Al-Wabel, M.I., Al-Omran, A., El-Naggar, A.H., Nadeem, M. and Usman, A.R.A. 2013. Pyrolysis temperature induced changes in characteristics and chemical composition of biochar produced from conocarpus wastes. Bioresource Technology 131, 374-379.

Al Afif, R., Anayah, S.S. and Pfeifer, C. 2020. Batch pyrolysis of cotton stalks for evaluation of biochar energy potential. Renewable Energy 147, 2250-2258.

Angın, D. 2013. Effect of pyrolysis temperature and heating rate on biochar obtained from pyrolysis of safflower seed press cake. Bioresource Technology 128, 593-597.

Anirudhan, T.S. and Sreekumari, S.S. 2011. Adsorptive removal of heavy metal ions from industrial effluents using activated carbon derived from waste coconut buttons. Journal of Environmental Sciences 23(12), 1989-1998.

Anwar, S., Shaukat, F. and Hussain, Z. 2010. IMPACT OF TRADE LIBERALIZATION ON EXPORT OF COTTON FROM PAKISTAN: A TIME SERIES ANALYSIS. Sarhad journal of Agriculture 26.

Arabi, Z., Rinklebe, J., El-Naggar, A., Hou, D., Sarmah, A.K. and Moreno-Jiménez, E. 2021. (Im)mobilization of arsenic, chromium, and nickel in soils via biochar: A meta-analysis. Environmental Pollution 286, 117199.

Azimi, A., Azari, A., Rezakazemi, M. and Ansarpour, M. 2017. Removal of Heavy Metals from Industrial Wastewaters: A Review. ChemBioEng Reviews 4(1), 37-59.

Barnhart, J. 1997. Occurrences, Uses, and Properties of Chromium. Regulatory Toxicology and Pharmacology 26(1), S3-S7.

Benjamin, S. and Nishat, A.M. 2021. Impacts of tanneries wastewater on the vicinal flora of Sheikhupura and Kasur, Pakistan. Ovidius University Annals of Chemistry 32, 90-97.

1007 Boretti, A. and Rosa, L. 2019. Reassessing the projections of the World Water
1008 Development Report. npj Clean Water 2(1), 15.
1009 Chandra, S. and Bhattacharya, J. 2019. Influence of temperature and duration of pyrolysis
1010 on the property heterogeneity of rice straw biochar and optimization of pyrolysis
1011 conditions for its application in soils. Journal of Cleaner Production 215, 1123-
1012 1139.
1013 Chen, Y., Yang, H., Wang, X., Zhang, S. and Chen, H. 2012. Biomass-based pyrolytic
1014 polygeneration system on cotton stalk pyrolysis: Influence of temperature.
1015 Bioresource Technology 107, 411-418.
1016 Cherdchoo, W., Nithettham, S. and Charoenpanich, J. 2019. Removal of Cr(VI) from
1017 synthetic wastewater by adsorption onto coffee ground and mixed waste tea.
1018 Chemosphere 221, 758-767.
1019 Choi, Y.-K. and Kan, E. 2019. Effects of pyrolysis temperature on the physicochemical
1020 properties of alfalfa-derived biochar for the adsorption of bisphenol A and
1021 sulfamethoxazole in water. Chemosphere 218, 741-748.
1022 Choudhary, B. and Paul, D. 2018. Isotherms, kinetics and thermodynamics of hexavalent
1023 chromium removal using biochar. Journal of Environmental Chemical Engineering
1024 6(2), 2335-2343.
1025 Demirbas, A. 2004. Effects of temperature and particle size on bio-char yield from
1026 pyrolysis of agricultural residues. Journal of Analytical and Applied Pyrolysis
1027 72(2), 243-248.
1028 Dong, X., Ma, L.Q. and Li, Y. 2011. Characteristics and mechanisms of hexavalent
1029 chromium removal by biochar from sugar beet tailing. Journal of Hazardous
1030 Materials 190(1), 909-915.
1031 Elwakeel, K.Z., Elgarahy, A.M., Khan, Z.A., Almughamisi, M.S. and Al-Bogami, A.S.
1032 2020. Perspectives regarding metal/mineral-incorporating materials for water
1033 purification: with special focus on Cr(vi) removal. Materials Advances 1(6), 1546-
1034 1574.
1035 Ertani, A., Mietto, A., Borin, M. and Nardi, S. 2017. Chromium in Agricultural Soils and
1036 Crops: A Review. Water, Air, & Soil Pollution 228(5), 190.

1037 Famielec, S. and Wieczorek-Ciurowa, K. 2011. Waste from leather industry. Threats to
1038 the environment. Czasopismo Techniczne. Chemia 108(1-Ch), 43-48.
1039 Gao, L., Li, Z., Yi, W., Li, Y., Zhang, P., Zhang, A. and Wang, L. 2021. Impacts of
1040 pyrolysis temperature on lead adsorption by cotton stalk-derived biochar and
1041 related mechanisms. Journal of Environmental Chemical Engineering 9(4),
1042 105602.
1043 Gibb, H.J., Lees, P.S.J., Pinsky, P.F. and Rooney, B.C. 2000. Lung cancer among workers
1044 in chromium chemical production. American Journal of Industrial Medicine 38(2),
1045 115-126.
1046 Guo, X., Liu, A., Lu, J., Niu, X., Jiang, M., Ma, Y., Liu, X. and Li, M. 2020. Adsorption
1047 Mechanism of Hexavalent Chromium on Biochar: Kinetic, Thermodynamic, and
1048 Characterization Studies. ACS Omega 5(42), 27323-27331.
1049 Gupta, A., Sharma, V., Sharma, K., Kumar, V., Choudhary, S., Mankotia, P., Kumar, B.,
1050 Mishra, H., Moulick, A., Ekielski, A. and Mishra, P.K. 2021. A Review of
1051 Adsorbents for Heavy Metal Decontamination: Growing Approach to Wastewater
1052 Treatment. Materials (Basel) 14(16).
1053 Gupta, V.K., Agarwal, S. and Saleh, T.A. 2011. Chromium removal by combining the
1054 magnetic properties of iron oxide with adsorption properties of carbon nanotubes.
1055 Water Research 45(6), 2207-2212.
1056 Gupta, V.K., Pathania, D., Agarwal, S. and Sharma, S. 2013. Removal of Cr(VI) onto
1057 Ficus carica biosorbent from water. Environmental Science and Pollution Research
1058 20(4), 2632-2644.
1059 Hajizadeh, Z., Taheri-Ledari, R. and Asl, F.R. (2022) Heterogeneous Micro and Nanoscale
1060 Composites for the Catalysis of Organic Reactions. Maleki, A. (ed), pp. 33-51,
1061 Elsevier.
1062 Hu, J., Chen, C., Zhu, X. and Wang, X. 2009. Removal of chromium from aqueous
1063 solution by using oxidized multiwalled carbon nanotubes. Journal of Hazardous
1064 Materials 162(2), 1542-1550.
1065 Hu, X.-j., Wang, J.-s., Liu, Y.-g., Li, X., Zeng, G.-m., Bao, Z.-l., Zeng, X.-x., Chen, A.-w.
1066 and Long, F. 2011. Adsorption of chromium (VI) by ethylenediamine-modified

cross-linked magnetic chitosan resin: Isotherms, kinetics and thermodynamics. Journal of Hazardous Materials 185(1), 306-314.

Imran, M., Khan, Z.U.H., Iqbal, M.M., Iqbal, J., Shah, N.S., Munawar, S., Ali, S., Murtaza, B., Naeem, M.A. and Rizwan, M. 2020. Effect of biochar modified with magnetite nanoparticles and HNO(3) for efficient removal of Cr(VI) from contaminated water: A batch and column scale study. Environ Pollut 261, 114231.

Kamali, M., Appels, L., Kwon, E.E., Aminabhavi, T.M. and Dewil, R. 2021. Biochar in water and wastewater treatment - a sustainability assessment. Chemical Engineering Journal 420, 129946.

Kerur, S.S., Bandekar, S., Hanagadakar, M.S., Nandi, S.S., Ratnamala, G.M. and Hegde, P.G. 2021. Removal of hexavalent Chromium-Industry treated water and Wastewater: A review. Materials Today: Proceedings 42, 1112-1121.

Khulbe, K. and Matsuura, T. 2018. Removal of heavy metals and pollutants by membrane adsorption techniques. Applied water science 8(1), 1-30.

Kim, P., Johnson, A., Edmunds, C.W., Radosevich, M., Vogt, F., Rials, T.G. and Labbé, N. 2011. Surface Functionality and Carbon Structures in Lignocellulosic-Derived Biochars Produced by Fast Pyrolysis. Energy & Fuels 25(10), 4693-4703.

Kimbrough, D.E., Cohen, Y., Winer, A.M., Creelman, L. and Mabuni, C. 1999. A Critical Assessment of Chromium in the Environment. Critical Reviews in Environmental Science and Technology 29(1), 1-46.

Kummu, M., Guillaume, J.H.A., de Moel, H., Eisner, S., Flörke, M., Porkka, M., Siebert, S., Veldkamp, T.I.E. and Ward, P.J. 2016. The world's road to water scarcity: shortage and stress in the 20th century and pathways towards sustainability. Scientific Reports 6(1), 38495.

Kuppusamy, S., Thavamani, P., Megharaj, M., Venkateswarlu, K., Lee, Y.B. and Naidu, R. 2016. Potential of Melaleuca diosmifolia leaf as a low-cost adsorbent for hexavalent chromium removal from contaminated water bodies. Process Safety and Environmental Protection 100, 173-182.

Lee, Y., Park, J., Ryu, C., Gang, K.S., Yang, W., Park, Y.-K., Jung, J. and Hyun, S. 2013. Comparison of biochar properties from biomass residues produced by slow pyrolysis at 500°C. Bioresource Technology 148, 196-201.

Li, H.-J., Fan, W.-Z., Pan, H.-H., Wang, C.-W., Qian, J. and Zhao, Q.-Z. 2017. Fabrication of "petal effect" surfaces by femtosecond laser-induced forward transfer. Chemical Physics Letters 667, 20-24.

Li, M., Liu, Q., Guo, L., Zhang, Y., Lou, Z., Wang, Y. and Qian, G. 2013. Cu(II) removal from aqueous solution by Spartina alterniflora derived biochar. Bioresource Technology 141, 83-88.

Liang, M., Ding, Y., Zhang, Q., Wang, D., Li, H. and Lu, L. 2020. Removal of aqueous Cr(VI) by magnetic biochar derived from bagasse. Scientific Reports 10(1), 21473.

Liu, Z., Niu, W., Chu, H., Zhou, T. and Niu, Z. 2018. Effect of the Carbonization Temperature on the Properties of Biochar Produced from the Pyrolysis of Crop Residues. BioResources 13.

López-Maldonado, E.A., Oropeza-Guzman, M.T., Jurado-Baizaval, J.L. and Ochoa-Terán, A. 2014. Coagulation–flocculation mechanisms in wastewater treatment plants through zeta potential measurements. Journal of Hazardous Materials 279, 1-10.

Lunk, H.-J. 2015. Discovery, properties and applications of chromium and its compounds. ChemTexts 1.

Ma, F., Zhao, B. and Diao, J. 2019a. Synthesis of magnetic biochar derived from cotton stalks for the removal of Cr(VI) from aqueous solution. Water Science and Technology 79(11), 2106-2115.

Ma, H., Yang, J., Gao, X., Liu, Z., Liu, X. and Xu, Z. 2019b. Removal of chromium (VI) from water by porous carbon derived from corn straw: Influencing factors, regeneration and mechanism. Journal of Hazardous Materials 369, 550-560.

Ma, Y., Liu, W.-J., Zhang, N., Li, Y.-S., Jiang, H. and Sheng, G.-P. 2014. Polyethylenimine modified biochar adsorbent for hexavalent chromium removal from the aqueous solution. Bioresource Technology 169, 403-408.

Makavana, J., Sarsavadia, P. and Chauhan, P. 2020. Effect of Pyrolysis Temperature and Residence Time on Bio-char Obtained from Pyrolysis of Shredded Cotton Stalk. International Research Journal of Pure and Applied Chemistry, 10-28.

Mdlovu, N.V., Lin, K.-S., Chen, Z.-W., Liu, Y. and Mdlovu, N.B. 2020. Treatment of simulated chromium-contaminated wastewater using polyethylenimine-modified

zero-valent iron nanoparticles. Journal of The Taiwan Institute of Chemical Engineers 108, 92-101.

Mohan, D., Rajput, S., Singh, V.K., Steele, P.H. and Pittman, C.U. 2011. Modeling and evaluation of chromium remediation from water using low cost bio-char, a green adsorbent. Journal of Hazardous Materials 188(1), 319-333.

Mortazavian, S., An, H., Chun, D. and Moon, J. 2018. Activated carbon impregnated by zero-valent iron nanoparticles (AC/nZVI) optimized for simultaneous adsorption and reduction of aqueous hexavalent chromium: Material characterizations and kinetic studies. Chemical Engineering Journal 353, 781-795.

Mulyanti, R. and Susanto, H. 2018. Wastewater treatment by nanofiltration membranes. IOP Conference Series: Earth and Environmental Science 142, 012017.

Nassar, M.M. and MacKay, G. 1984. Mechanism of thermal decomposition of lignin. Wood and Fiber Science, 441-453.

Neelam, A., Alamgir, A. and Kanwal, H. 2018. Determination of chromium in the tannery wastewater, Korangi, Karachi. International Journal of Environmental Sciences & Natural Resources 15(4), 122-125.

Nriagu, J.O. and Pacyna, J.M. 1988. Quantitative assessment of worldwide contamination of air, water and soils by trace metals. Nature 333(6169), 134-139.

Othmani, A., Magdouli, S., Senthil Kumar, P., Kapoor, A., Chellam, P.V. and Gökkuş, Ö. 2022. Agricultural waste materials for adsorptive removal of phenols, chromium (VI) and cadmium (II) from wastewater: A review. Environmental Research 204, 111916.

Owlad, M., Aroua, M.K., Daud, W.A.W. and Baroutian, S. 2009. Removal of Hexavalent Chromium-Contaminated Water and Wastewater: A Review. Water, Air, and Soil Pollution 200(1), 59-77.

Pagilla, K.R. and Canter, L.W. 1999. Laboratory Studies on Remediation of Chromium-Contaminated Soils. Journal of Environmental Engineering 125(3), 243-248.

Rafique, M.I., Usman, A.R.A., Ahmad, M. and Al-Wabel, M.I. 2021. Immobilization and mitigation of chromium toxicity in aqueous solutions and tannery waste-contaminated soil using biochar and polymer-modified biochar. Chemosphere 266, 129198.

Reddy, C.V., Reddy, I.N., Koutavarapu, R., Reddy, K.R., Saleh, T.A., Aminabhavi, T.M. and Shim, J. 2022. Novel edge-capped ZrO2 nanoparticles onto V2O5 nanowires for efficient photosensitized reduction of chromium (Cr (VI)), photoelectrochemical solar water splitting, and electrochemical energy storage applications. Chemical Engineering Journal 430, 132988.

Renu, Agarwal, M. and Singh, K. 2016. Heavy metal removal from wastewater using various adsorbents: a review. Journal of Water Reuse and Desalination 7(4), 387-419.

Riaz, A. and Zia, A. 2020. Appraisal of Chromium Contents from Different Tanneries and Drains of Sialkot. Pakistan Journal of Scientific & Industrial Research Series A: Physical Sciences 63(2), 112-117.

Sakhiya, A.K., Anand, A. and Kaushal, P. 2020. Production, activation, and applications of biochar in recent times. Biochar 2(3), 253-285.

Shakya, A. and Agarwal, T. 2019. Removal of Cr(VI) from water using pineapple peel derived biochars: Adsorption potential and re-usability assessment. Journal of Molecular Liquids 293, 111497.

Shanker, A.K., Cervantes, C., Loza-Tavera, H. and Avudainayagam, S. 2005. Chromium toxicity in plants. Environment International 31(5), 739-753.

Shen, Y.-S., Wang, S.-L., Tzou, Y.-M., Yan, Y.-Y. and Kuan, W.-H. 2012. Removal of hexavalent Cr by coconut coir and derived chars – The effect of surface functionality. Bioresource Technology 104, 165-172.

Sikder, M.T., Kikuchi, T., Suzuki, J., Hosokawa, T., Saito, T. and Kurasaki, M. 2013. Removal of Cadmium and Chromium Ions Using Modified α, β, and γ-Cyclodextrin Polymers. Separation Science and Technology 48(4), 587-597.

Sinha, R., Kumar, R., Abhishek, K., Shang, J., Bhattacharya, S., Sengupta, S., Kumar, N., Singh, R.K., Mallick, J., Kar, M. and Sharma, P. 2022a. Single-step synthesis of activated magnetic biochar derived from rice husk for hexavalent chromium adsorption: Equilibrium mechanism, kinetics, and thermodynamics analysis. Groundwater for Sustainable Development 18, 100796.

Sinha, R., Kumar, R., Sharma, P., Kant, N., Shang, J. and Aminabhavi, T.M. 2022b. Removal of hexavalent chromium via biochar-based adsorbents: State-of-the-art,

challenges, and future perspectives. Journal of Environmental Management 317, 115356.

Song, W., Gao, B., Zhang, T., Xu, X., Huang, X., Yu, H. and Yue, Q. 2015. High-capacity adsorption of dissolved hexavalent chromium using amine-functionalized magnetic corn stalk composites. Bioresource Technology 190, 550-557.

Tański, T., Matysiak, W., Krzemiński, Ł., Jarka, P. and Gołombek, K. 2017. Optical properties of thin fibrous PVP/SiO2 composite mats prepared via the sol-gel and electrospinning methods. Applied Surface Science 424, 184-189.

Tariq, M.A., Nadeem, M., Iqbal, M.M., Imran, M., Siddique, M.H., Iqbal, Z., Amjad, M., Rizwan, M. and Ali, S. 2020. Effective sequestration of Cr (VI) from wastewater using nanocomposite of ZnO with cotton stalks biochar: modeling, kinetics, and reusability. Environmental Science and Pollution Research 27(27), 33821-33834.

Tomczyk, A., Sokołowska, Z. and Boguta, P. 2020. Biochar physicochemical properties: pyrolysis temperature and feedstock kind effects. Reviews in Environmental Science and Bio/Technology 19(1), 191-215.

Tong, X.-j., Li, J.-y., Yuan, J.-h. and Xu, R.-k. 2011. Adsorption of Cu(II) by biochars generated from three crop straws. Chemical Engineering Journal 172(2), 828-834.

Tytłak, A., Oleszczuk, P. and Dobrowolski, R. 2015. Sorption and desorption of Cr(VI) ions from water by biochars in different environmental conditions. Environmental Science and Pollution Research 22(8), 5985-5994.

Usman, A.R.A., Abduljabbar, A., Vithanage, M., Ok, Y.S., Ahmad, M., Ahmad, M., Elfaki, J., Abdulazeem, S.S. and Al-Wabel, M.I. 2015. Biochar production from date palm waste: Charring temperature induced changes in composition and surface chemistry. Journal of Analytical and Applied Pyrolysis 115, 392-400.

Van der Bruggen, B., Vandecasteele, C., Gestel, T., Doyen, W. and Leysen, R. 2003. A Review of Pressure-Driven Membrane Processes in Wastewater Treatment and Drinking Water Production. Environmental Progress 22, 46-56.

Wang, B., Li, F. and Wang, L. 2020a. Enhanced hexavalent chromium (Cr(VI)) removal from aqueous solution by Fe–Mn oxide-modified cattail biochar: adsorption characteristics and mechanism. Chemistry and Ecology 36(2), 138-154.

Wang, H., Zhang, M. and Lv, Q. 2019. Removal Efficiency and Mechanism of Cr(VI) from Aqueous Solution by Maize Straw Biochars Derived at Different Pyrolysis Temperatures. Water 11(4).

Wang, S.-y., Tang, Y.-k., Li, K., Mo, Y.-y., Li, H.-f. and Gu, Z.-q. 2014. Combined performance of biochar sorption and magnetic separation processes for treatment of chromium-contained electroplating wastewater. Bioresource Technology 174, 67-73.

Wang, Y., Wu, H., Sárossy, Z., Dong, C. and Glarborg, P. 2017. Release and transformation of chlorine and potassium during pyrolysis of KCl doped biomass. Fuel 197, 422-432.

Wang, Z., Shu, X., Zhu, H., Xie, L., Cheng, S. and Zhang, Y. 2020b. Characteristics of biochars prepared by co-pyrolysis of sewage sludge and cotton stalk intended for use as soil amendments. Environmental Technology 41(11), 1347-1357.

Xiao, X., Chen, Z. and Chen, B. 2016. H/C atomic ratio as a smart linkage between pyrolytic temperatures, aromatic clusters and sorption properties of biochars derived from diverse precursory materials. Scientific Reports 6(1), 22644.

Xu, D., Sun, T., Jia, H., Sun, Y. and Zhu, X. 2022. The performance and mechanism of Cr(VI) adsorption by biochar derived from Potamogeton crispus at different pyrolysis temperatures. Journal of Analytical and Applied Pyrolysis 167, 105662.

Yang, Y., Zhang, Y., Wang, G., Yang, Z., Xian, J., Yang, Y., Li, T., Pu, Y., Jia, Y., Li, Y., Cheng, Z., Zhang, S. and Xu, X. 2021. Adsorption and reduction of Cr(VI) by a novel nanoscale FeS/chitosan/biochar composite from aqueous solution. Journal of Environmental Chemical Engineering 9(4), 105407.

Yin, R., Liu, R., Mei, Y., Fei, W. and Sun, X. 2013. Characterization of bio-oil and bio-char obtained from sweet sorghum bagasse fast pyrolysis with fractional condensers. Fuel 112, 96-104.

Yusuff, A.S., Lala, M.A., Thompson-Yusuff, K.A. and Babatunde, E.O. 2022. ZnCl2-modified eucalyptus bark biochar as adsorbent: preparation, characterization and its application in adsorption of Cr(VI) from aqueous solutions. South African Journal of Chemical Engineering 42, 138-145.

Zhang, J., Chen, S., Zhang, H. and Wang, X. 2017. Removal behaviors and mechanisms of hexavalent chromium from aqueous solution by cephalosporin residue and derived chars. Bioresource Technology 238, 484-491.

Zhang, X., Lv, L., Qin, Y., Xu, M., Jia, X. and Chen, Z. 2018a. Removal of aqueous Cr(VI) by a magnetic biochar derived from Melia azedarach wood. Bioresource Technology 256, 1-10.

Zhang, X., Zhang, L. and Li, A. 2018b. Eucalyptus sawdust derived biochar generated by combining the hydrothermal carbonization and low concentration KOH modification for hexavalent chromium removal. Journal of Environmental Management 206, 989-998.

Zhitkovich, A. 2011. Chromium in Drinking Water: Sources, Metabolism, and Cancer Risks. Chemical Research in Toxicology 24(10), 1617-1629.

Zhong, Z., Yu, G., Mo, W., Zhang, C., Huang, H., Li, S., Gao, M., Lu, X., Zhang, B. and Zhu, H. 2019. Enhanced phosphate sequestration by Fe(iii) modified biochar derived from coconut shell. RSC Advances 9(18), 10425-10436.

Zhou, L., Liu, Y., Liu, S., Yin, Y., Zeng, G., Tan, X., Hu, X., Hu, X., Jiang, L., Ding, Y., Liu, S. and Huang, X. 2016. Investigation of the adsorption-reduction mechanisms of hexavalent chromium by ramie biochars of different pyrolytic temperatures. Bioresource Technology 218, 351-359.